A Comprehensive Kinetic Mechanism for CO, CH_2O, and CH_3OH Combustion

JUAN LI,[1] ZHENWEI ZHAO,[1] ANDREI KAZAKOV,[1] MARCOS CHAOS,[1] FREDERICK L. DRYER,[1] JAMES J. SCIRE, JR.[2]

[1]*Department of Mechanical and Aerospace Engineering, Princeton University, Princeton,* NJ 08544
[2]*Advanced Fuel Research, Inc., East Hartford,* CT 06108

Received 27 May 2006; revised 18 September 2006; accepted 3 October 2006

DOI 10.1002/kin.20218
Published online in Wiley InterScience (www.interscience.wiley.com).

ABSTRACT: New experimental profiles of stable species concentrations are reported for formaldehyde oxidation in a variable pressure flow reactor at initial temperatures of 850–950 K and at constant pressures ranging from 1.5 to 6.0 atm. These data, along with other data published in the literature and a previous comprehensive chemical kinetic model for methanol oxidation, are used to hierarchically develop an updated mechanism for $CO/H_2O/H_2/O_2$, CH_2O, and CH_3OH oxidation. Important modifications include recent revisions for the hydrogen–oxygen submechanism (Li et al., *Int J Chem Kinet* 2004, 36, 565), an updated submechanism for methanol reactions, and kinetic and thermochemical parameter modifications based upon recently published information. New rate constant correlations are recommended for $CO + OH = CO_2 + H$ (R23) and $HCO + M = H + CO + M$ (R24), motivated by a new identification of the temperatures over which these rate constants most affect laminar flame speed predictions (Zhao et al., *Int J Chem Kinet* 2005, 37, 282). The new weighted least-squares fit of literature experimental data for (R23) yields $k_{23} = 2.23 \times 10^5 T^{1.89} \exp(583/T)$ $cm^3/mol/s$ and reflects significantly lower rate constant values at low and intermediate temperatures in comparison to another recently recommended correlation and theoretical predictions. The weighted least-squares fit of literature results for (R24) yields $k_{24} = 4.75 \times 10^{11} T^{0.66} \exp(-7485/T)$ $cm^3/mol/s$, which predicts values within uncertainties of both prior and new (Friedrichs et al., *Phys Chem Chem Phys* 2002, 4, 5778; DeSain et al., *Chem Phys Lett* 2001, 347, 79) measurements. Use of either of the data correlations reported in Friedrichs et al. (2002) and DeSain et al. (2001) for this reaction significantly degrades laminar flame speed predictions for oxygenated fuels as well as for other hydrocarbons. The present C_1/O_2 mechanism compares favorably against a wide range of experimental conditions for laminar premixed flame speed, shock tube ignition delay, and flow reactor species time history data at each level of hierarchical development. Very good agreement of the model predictions with all of the experimental measurements is demonstrated.
 Int J Chem Kinet 39: 109–136, 2007

Correspondence to: Frederick L. Dryer; e-mail: fldryer@princeton.edu.

Present address of J. Li: Praxair, Inc., Tonawanda, NY 14221.

Present address of A. Kazakov: Thermodynamics Research Center, NIST, Boulder, CO 80305.

Contract grant sponsor: Chemical Sciences, Geosciences and Biosciences Division, Office of Basic Energy Sciences, Office of Science, U.S. Department of Energy.

Contract grant number: DE-FG02-86ER13503.

INTRODUCTION

The hierarchical nature of hydrocarbon oxidation kinetics and the importance of small molecule and radical kinetics in controlling the oxidation of larger carbon number species are well-established notions [1,2]. The hydrogen–oxygen kinetic submechanism [2] controls the most reactive radical pool composition of H, OH, O, and HO_2 that attack the primary fuel. Carbon monoxide is a major intermediate species, and its conversion to CO_2 is responsible for a significant fraction of the exothermicity accompanying hydrocarbon oxidation. It has been shown (e.g., [2,3]) that nearly all carbon atoms bonded to one another, to hydrogen atoms, or hydroxyl groups are converted to CO through formaldehyde (CH_2O) and/or formyl radicals (HCO). Formyl radicals are a major source of H atoms and HO_2 radicals in larger carbon number hydrocarbon combustion.

Methanol (CH_3OH), the simplest alcohol, converts to CO through CH_2O reactions and introduces additional species, particularly CH_2, CH_3, CH_3O, and CH_2OH [4]. Over almost all conditions of practical interest, methanol combustion produces CH_3 in such minor concentrations that no C_2 hydrocarbon species are formed and, hence, no sooting occurs. The collection of kinetic phenomena involved in hydrogen/oxygen, carbon monoxide, formaldehyde, and methanol is therefore a representative of the small radical pool interactions that couple with methyl radical and higher carbon number species and radicals in hydrocarbon combustion systems.

Detailed mechanisms for H_2, CO, CH_2O, and CH_3OH combustion are also individually of practical importance. Hydrogen kinetic properties have long been of interest in terms of safety, given the major use of hydrogen in chemical synthesis and fuel refining. The proposed transition to a hydrogen energy economy further emphasizes the need to understand hydrogen safety issues [e.g., 5,6] as well as hydrogen combustion under mild combustion conditions and with very high-exhaust gas recirculation. Carbon monoxide and formaldehyde are primary pollutant species emitted from many combustion systems and are important in reforming chemistry to produce hydrogen from hydrocarbons, as well as in atmospheric chemistry, toxicity, and carcinogen assessments and analyses. Methanol is used as an oxygenate additive in gasoline and is also an attractive alternative to traditional transportation fuels because of its nonsooting characteristics, its facile synthesis from a wide variety of feedstocks, and its possible interim role as a hydrogen carrier for fuel cell applications.

The combustion chemistry of each of the above species has been extensively studied previously. Experimental data exist in the literature from laminar flame, shock tube, flow reactor, and static reactor experiments, collectively covering a wide range of initial temperature, pressure, and equivalence ratio. Our group has had a long involvement in studying these small molecule kinetics in flow reactors (Yetter et al. [7,8]; Hochgreb and Dryer [9]; Kim et al. [10], Norton and Dryer [11], Held and Dryer [4,12], Mueller et al. [13–17]). We have previously developed comprehensive mechanisms for CO [8], CH_2O [9], and CH_3OH [4], and our recent work on updating and developing a comprehensive mechanism for hydrogen–oxygen [18] that includes advances in chemical kinetic rate and thermochemical information as well as validation data sources points to the need to similarly revisit and update our prior work on carbon monoxide, formaldehyde, and methanol kinetics. While the flow reactor data we have previously published for hydrogen, carbon monoxide, and methanol systems, each covering a very wide range of pressures, our prior work on formaldehyde oxidation was limited to atmospheric pressure studies [9]. In that work, chemical analyses were conducted using offline gas chromatography, an analytical method with potentially higher uncertainties than can be achieved using the Fourier transform infrared (FTIR) online analytical methods available today. Formaldehyde oxidation obtained in a variable pressure flow reactor (VPFR) at initial temperatures of 850–950 K and constant pressures ranging from 1.5 to 6.0 atm to expand the range of validation conditions. Moreover, new experiments in other venues, especially for CH_2O oxidation, have appeared in the literature using shock tubes [19–22] and laminar premixed flames [23]. In addition, there have been some elementary kinetic publications further addressing the important reactions involved in the C_1 oxidation system (e.g., [19,24,25]).

Utilizing our recent work on hydrogen/oxygen kinetics [18], and updating the CO/O_2, CH_2O/O_2, and CH_3OH/O_2 mechanisms with more recent kinetic and thermochemical information, a comprehensive mechanism has been hierarchically developed [26] that satisfactorily reproduces new experimental targets as well as those utilized in the original mechanism studies appearing in [4,8,9]. This paper reports the key features of the updated mechanism, summarizes the comparisons of predictions with experimental targets as performed in [26], and augments these earlier comparisons using the results with some additional, recently published, kinetic measurements and experimental validation data.

EXPERIMENTAL METHODS

The new experiments on formaldehyde oxidation reported here were conducted in the Princeton variable pressure flow reactor [27]. Detailed information on the VPFR instrumentation and experimental methodology can be found in other publications [28], and only a brief description is given here.

Carrier gas (N_2 in this study) is heated by a pair of electrical resistance heaters and directed into a reactor duct. Oxygen is also introduced at the duct entrance. The carrier gas/oxygen mixture flows around a baffle plate into a gap serving as the entrance to a diffuser. The vaporized fuel (trioxane with water in this study) flows into the center tube of a fuel injector and injects radially outward into the gap where it rapidly mixes with the carrier gas and oxygen. The reacting mixture exits the diffuser into a constant area test section. Near the exit of the test section, a sampling probe is positioned on the reactor centerline to continuously extract and convectively quench a small percentage of the flow. At the same axial location, the local reaction gas temperature is measured with a type R thermocouple accurate to ± 3 K.

The sample gas flows via heated Teflon lines to analytical equipment including a FTIR spectrometer, an electrochemical O_2 analyzer, and a pair of nondispersive infrared analyzers for CO and CO_2. Other stable species of interest (e.g., CH_2O, H_2O) are measured continuously online using FTIR spectrometry. The measurement uncertainties for the data reported here are O_2:$\pm$2%, CO:$\pm$2%, CO_2:$\pm$2%, CH_2O:$\pm$3%, and H_2O:$\pm$6% of reading.

The distance between the point of fuel injection and the sampling position is varied by moving the fuel vapor injector probe (with attached mixer/diffuser assembly) relative to the fixed sampling location. Mean axial velocity measurements along the centerline of the reactor are used to correlate distance with residence time. By these means, profiles of stable species versus residence time can be determined experimentally. The uncertainty in the residence time is approximately 5%.

In the present experiments, formaldehyde monomer was generated through the decomposition of 1,3,5-trioxane. Hochgreb and Dryer [9] also employed this technique in their atmospheric pressure flow reactor (APFR) experiments. Trioxane decomposition proceeds by the concerted rupture of the three C—O bonds to form three formaldehyde molecules [9,29]. Using gas chromatography, it was experimentally verified that CH_2O is the only product of trioxane decomposition, and trioxane decomposition is much faster than the subsequent reaction of formaldehyde at flow reactor conditions. For modeling purposes, 1 mol of trioxane reactant could therefore be replaced by 3 mol of formaldehyde.

In earlier work, [9,29], trioxane was melted and delivered as a liquid to the evaporator of a prior APFR. A similar methodology would have required a complex modification of the present reactor, and a different approach to deliver trioxane to the reactor was utilized. At 18°C, the solubility of trioxane in water is 17.2 g/100 mL [30]. Trioxane was dissolved in distilled water, and the unheated solution was volumetrically metered to a liquid vaporizer system located within the VPFR pressure shell and at the immediate entrance to the fuel vapor injector probe. The metered liquid flow was gas-blast atomized using heated nitrogen, and the nitrogen, water vapor, and trioxane vapor mixture was then injected into the reactor at the mixing location with hot carrier gas. It was verified that the decomposition rate of trioxane at the conditions of the reported experiments led to immediate formation of monomer during the injection and mixing process, well upstream of the radially uniform reaction region where the reported data were obtained. Due to heat addition limitations for the hot nitrogen used to vaporize the liquid reactant flow and the solubility limit of trioxane in water, the maximum initial CH_2O mole fraction investigated was limited to 500 ppm. Other than this limitation, the use of water to deliver the trioxane did not significantly affect the experiments, as the amount of water added was included in the kinetic modeling comparisons.

A series of moist formaldehyde oxidation experiments were conducted in the VPFR at initial temperatures of 850–950 K and in the pressure range of 1.5–6.0 atm. For all of the experiments, the total carbon and oxygen balances experimentally determined at each residence time were within 4% of the specified input. The nearly identical total carbon and oxygen concentrations at each sampling location not only provide verification of the experimental measurements but also imply that any other carbon- or oxygen-containing stable species present were only in negligible quantities. Although formic acid has been observed using these same diagnostics in VPFR experiments on methanol [4] and dimethyl ether [31] oxidation, none was detected in the present experiments on formaldehyde oxidation. This is most likely the result of the very low fuel concentrations studied here, and that formic acid would be expected to be below detection limits.

UPDATED KINETIC MECHANISMS FOR CO, CH_2O, AND CH_3OH COMBUSTION

We used a slightly modified version of the methanol mechanism published by Held and Dryer [4] as a

starting point in developing the present mechanism.* In the course of the present work, a number of thermochemical parameters and rate constant correlations were modified to reflect more recent kinetic information. The revised H_2/O_2 submechanism is discussed in detail and validated against a large set of hydrogen/oxygen targets in a separate publication [18], and this submechanism is absorbed without further modifications in the present work. Revisions included the use of the heat of formation of OH recommended by Ruscic et al. [33], which is in very good agreement with recent experimental results [34]. For the current work, we utilized 3.0 kcal/mol as the standard heat of formation of HO_2 at 298.15 K [35]. Very recently, Ruscic et al. [36] have updated this heat of formation to 2.94 ± 0.06 kcal/mol. This change makes no significant difference in the level of comparison of computations with the targets utilized in the present work.

In addition to revising the components associated with the hydrogen–oxygen submechanism, the following revisions were also adopted over the course of this work.

Thermochemical Data for CH_2OH

The thermochemical properties of CH_2OH, including enthalpy of formation, standard entropy, and heat capacity at different temperatures, were updated to those reported by Johnson and Hudgens [37]. The data of Johnson and Hudgens also agree well with another recent IUPAC evaluation by Ruscic et al. [38]. These thermodynamic properties were fitted with a 14-coefficient polynomial [39].

$CO + OH = CO_2 + H$ (R23)

This well-studied reaction is of critical importance to combustion modeling because it is the main pathway to convert CO to CO_2, the oxidation of CO is responsible for a major fraction of the energy release derived in oxidation of hydrocarbons, and CO_2 dissociation important in determining adiabatic flame temperatures as a function of pressure. The reaction proceeds through the formation of HOCO adducts and thus is pressure dependent, particularly at low temperatures [25,40]. Under most practical combustion conditions, however, the reaction can be treated as pressure-independent.

The rate of oxidation of $H_2/CO/O_2$ and moist CO mixtures is very sensitive to reaction (R23) [8]. Moreover, laminar flame speed predictions of hydrocarbons are strongly influenced by this reaction [41,42]. It is not surprising that targets such as shock tube ignition delay data or flow reactor data would constrain model parameters only over the particular range of temperature covered by the work. However, the temperature range over which laminar flame speed predictions are most sensitive to a particular elementary reaction has typically not been considered.

Recently, Zhao et al. [43] introduced a methodology to determine the temperature-dependent sensitivity of premixed laminar flame speeds to elementary rate constant and transport properties. Analyses were conducted by locally perturbing the parameter with a Gaussian function profile. The center of the Gaussian profile was moved with an assigned temperature mean, and the sensitivity of the predicted flame speed was determined as a function of the perturbation-assigned mean temperature. The analysis leads to the determination of a "temperature window" in which the predicted laminar flame speed is found to be most sensitive to perturbations in the particular parameter. The temperature sensitivity of laminar flames for hydrogen/carbon monoxide mixtures with respect to (R23) was used as an application demonstration. The predicted laminar flame speed was shown to be most sensitive to the specific rate of (R23) in the temperature range 300–1900 K (Fig. 1).

Recently, Yu [44], Troe [45], Zhu et al. [46], and Senosiain et al. [25] performed detailed Rice–Ramsperger–Kassel–Marcus (RRKM) calculations to model the temperature and pressure dependence of this reaction. Most of these correlations were primarily calibrated against high-temperature shock tube data and predict higher rates than experimental measurements at low to intermediate temperatures, as shown in Fig. 2 (the only exception being the results of Zhu et al. [46] which underpredict the majority of experimental data at the temperatures of interest). These temperatures include the temperature sensitivity window for CO laminar flame speed to this reaction. If one assumes that the theoretical fits misrepresent the specific rate of this reaction by comparison with the (presumably) more accurate experimental data at these temperatures, one would expect CO/H_2 flame speeds to be overpredicted with the reaction models based on these rate parameters. Indeed, as shown in Fig. 3, GRI-Mech 3.0 [47], which uses the values of Yu [44], overpredicts the experimentally measured CO/H_2/air laminar flame speeds of McLean et al. [48].

On the basis of the above considerations, we fit the entire body of experimentally measured rate constants

*In verifying the published mechanism, we found that the model reported in [4] resulted in calculated flame speeds that were much higher than those shown in the publication. Dr. Held [32] concurs that the flame speed calculations reported in the paper resulted from the slightly modified version of the reported mechanism, used as a basis in the current work.

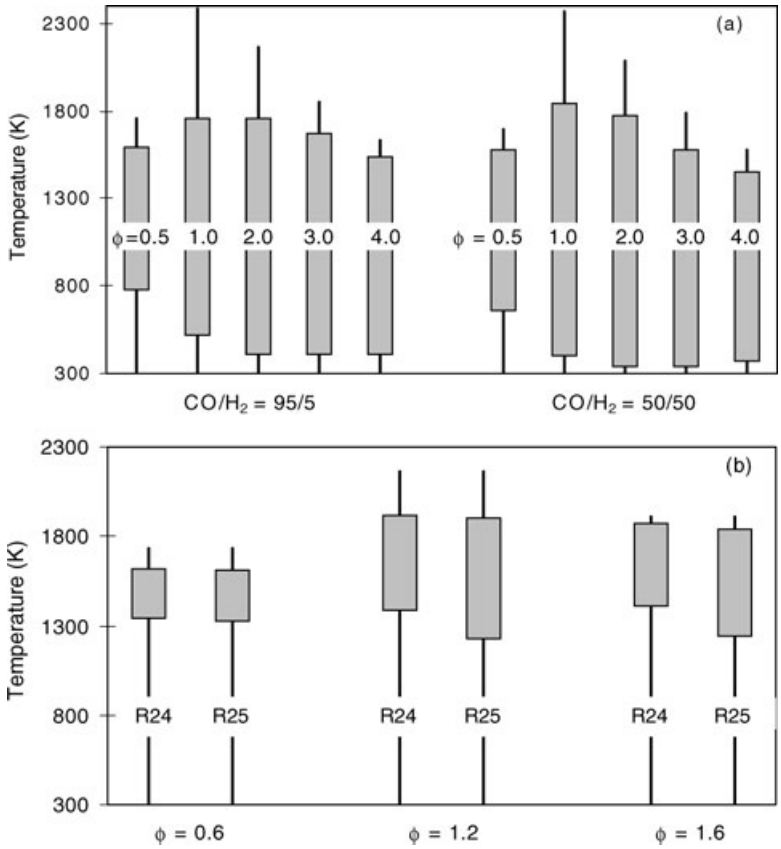

Figure 1 Sensitivity spectrum of reactions $CO + OH = CO_2 + H$, (R23), $HCO + M = H + CO + M$, (R24), and $HCO + O_2 = HO_2 + CO$, (R25), for a range of equivalence ratio predicted by the present C_1/O_2 kinetic mechanism. The figures are taken from Zhao et al. [43]. Figure (a) is the sensitivity spectrum of (R23) for ambient CO/H_2/air flames of two initial fuel compositions (95% $CO + 5\%$ H_2 and 50% $CO + 50\%$ H_2); (b) is that of (R24) and (R25) for ambient CH_3OH/air flames. Bars indicate the temperature range where the sensitivity is more than 10% of the maximum value, and lines represent the temperature span for the specific flame.

available in the literature [44,49–54] by the method of weighted least squares to obtain a more representative correlation of the experimental measurements of this rate constant. The sum of weighted squared errors

$$\Psi = \sum_{i=1}^{N} \left(\frac{\log k_{\exp}(T_i) - \log k(T_i)}{\sigma_i} \right)^2 \qquad (1)$$

is minimized by taking the rate constant, k, as

$$k_{23} = 10^{5.35\left(^{-0.39}_{+0.48}\right)} T^{1.89\left(^{+0.11}_{-0.14}\right)} \times \exp\left[583 \begin{pmatrix} +82 \\ -106 \end{pmatrix} \Big/ T \right] \text{cm}^3/\text{mol/s} \qquad (2)$$

In Eq. (1), $k_{\exp}$ is the rate constant measured experimentally at temperature T_i, and σ_i is the absolute error of $\log k_{\exp}$ at T_i. Equation (2) was used as the rate constant of reaction (R23) in this study. The values shown in parentheses in Eq. (2) are the 95% confidence intervals of the fitted parameters.

Figure 2 shows the comparison of this expression with literature results, including those of Lissianski et al. [54] which in the current study were recalculated based on the present thermochemical data and the rate constant of the reverse reaction of (R23) provided in the original paper [54]. The new correlation predicts specific rate constant values in close agreement with those obtained from the correlation of Yu et al. [55] (within 6% at 800–3500 K) derived by fitting their high-temperature experimental measurements in a shock tube. In the temperature window of 800–2000 K, predictions from the new expression agree well (within 10%) with those of Troe [45] at 1 atm, while they are about 20% lower than the theoretical predictions of Yu [44] and Senosiain et al. [25] at 1 atm.

Very recently, and since the thesis research on this work [26], another theoretical treatment of reaction

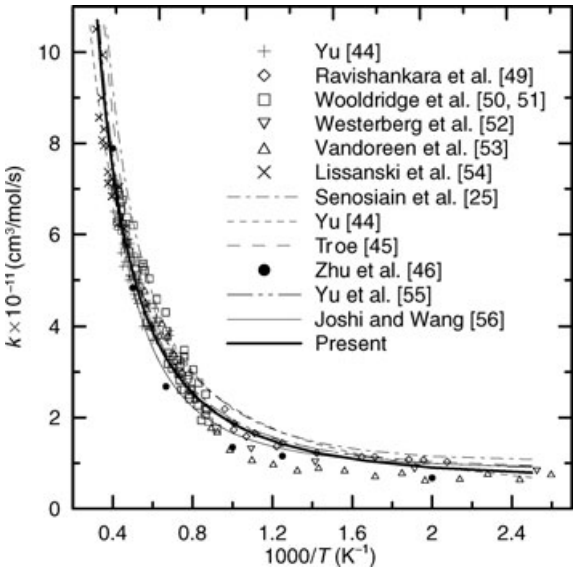

Figure 2 Rate constant of reaction $CO + OH \rightarrow CO_2 + H$ (R23). Symbols are experimental data (except for atmospheric pressure theoretical results of Zhu et al. [46]). Lines are the recommendations of Yu [44], Troe [45], Yu et al. [55] at 1 atm, Senosiain et al. [25] at 1 atm, Joshi and Wang [56] at the low-pressure limit, and that used in the present C_1 mechanism (Eq. (2)).

(R23) has appeared in the literature [56]. Joshi and Wang [56] have pointed out that consideration of both cis- and trans-isomeric forms of HOCO adduct as well as hindered rotation connecting the two (ignored in prior theoretical studies) leads to significant changes in the predicted thermal rate constant for reaction (R23). The resulting expression recommended by these authors is also plotted in Fig. 2. As can be seen, their result is significantly lower at the intermediate temperatures of interest than the earlier theoretical predictions. Joshi and Wang have also indicated that "the treatment of the title reaction (R23) remains semi-empirical as more than one different model can satisfactory reproduce a wide range of data." The present empirical fit (Eq. (2)) is approximately half-way between the theoretical results of Senosiain et al. [25] and the new results of Joshi and Wang [56].

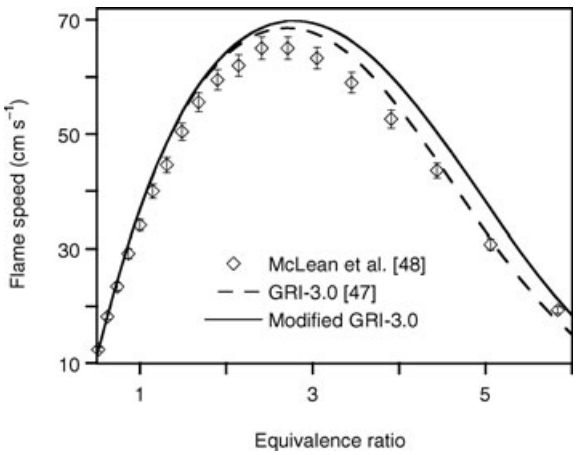

Figure 3 Laminar flame speed of CO/H_2/air mixtures at 298 K and 1 atm. The fuel composition is 95% CO and 5% H_2. Symbols—experimental data of McLean et al. [48]; dotted line—predictions of GRI-Mech 3.0 [47]; solid line—predictions of GRI-Mech 3.0 modified by replacing the rate coefficients of reactions (R24) and (R25) with the recommendations of Friedrichs et al. [19] and DeSain et al. [24], respectively.

$HCO + M = H + CO + M$ (R24) and $HCO + O_2 = HO_2 + CO$ (R25)

Both the unimolecular decomposition and abstraction reactions of formyl radicals are the main pathways to generate CO during the high-temperature combustion of hydrocarbons. Because the H atom in HCO is very weakly bound, the dissociation reaction (R24) competes strongly with the H-abstraction reactions from HCO by H, OH, and O_2. Timonen et al. [57,58] directly measured the rate constant of reactions (R24) and (R25) in a heated tubular reactor below 832 and 713 K, respectively. More recently, Friedrichs et al. [19] detected HCO in a shock tube for the first time by using frequency-modulated spectroscopy. Based on a reaction mechanism primarily derived from GRI-Mech 3.0 [47], the rate constant of reaction (R24) was estimated by fitting the experimental HCO profiles at 835–1230 K [19]. The work of Friedrichs et al. [19] infers that the rate of (R24) is about two times lower than the measurements of Timonen et al. [57]. DeSain et al. [24] also studied reaction (R25) at 296–673 K experimentally and reported a temperature-independent rate constant, which is about two times lower than that of Timonen et al. [58] at 1000 K.

In a flow reactor study of $CH_2O/NO/O_2$, Glarborg et al. [59] adopted the expressions of Friedrichs et al. [19] and DeSain et al. [24] for reactions (R24) and (R25), respectively, in a revised kinetic mechanism, which predicted their flow reactor measurements reasonably well. Incorporating these expressions within the present mechanism also results in as good agreement with the flow reactor experiments of [9] as achieved using the recommendations of Timonen et al. [57,58]. Closer inspection, however, reveals that the ratio k_{24}/k_{25} for the new correlations is almost the same as that used previously, and that the CH_2O/O_2 system predictions under flow reactor conditions are sensitive to this ratio, rather than to the absolute magnitudes of the individual specific rate constants [9]. On the other hand, premixed laminar flame speeds of

hydrocarbons, particularly those of simple oxygenates such as formaldehyde and methanol, are very sensitive to the absolute rates of (R24) and (R25) (e.g., [4]). Using the recommendations of [19,24] yields substantially different flame speed predictions from those obtained with the correlations of Timonen et al. [57,58]. Attempting to compensate for these discrepancies by combinatorial modifications of other elementary rate constants degrades the quality of predictions against other experimental targets.

Figure 3 compares the experimental flame speeds of CO/H_2/air mixtures [48] with model predictions of GRI-Mech-3.0 [47] and with the predictions of a "modified" GRI-Mech-3.0 in which the rate coefficient correlations for reactions (R24) and (R25) are replaced by the recommendations of Friedrichs et al. [19] and DeSain et al. [24], respectively. The overall uncertainty of the experimental flame speeds was reported to be ±3% [48]. Obviously, the predictions of the modified mechanism are significantly degraded in comparison to those using the original mechanism and depart substantially from the experiments, particularly at fuel rich equivalence ratios. Similar behavior was observed for the laminar flame speeds of other hydrocarbon/air mixtures, particularly those for CH_3OH/air and C_2H_5OH/air mixtures. In further demonstration of the novel method of temperature-dependent sensitivity analysis, Zhao et al. [43] showed that 1300–2000 and 1200–1900 K are the temperature windows where hydrocarbon laminar flame speed predictions are most sensitive to reaction (R24) and (R25), respectively (Fig. 1). These temperature ranges are well above the range of conditions of both the recent measurements of [19,24], and the earlier measurements of Timonen et al. [57,58]. Extrapolation of the rate constant correlations recommended in [19,24] yields substantially lower values for the rate constants within these temperature ranges than extrapolation of those recommended in [57,58]. As a result of these analyses, the correlations recommended previously by Timonen et al. [57] and those in [19,24] were not adopted in this study even though the reported rate measurements [19,24] appear to have smaller estimated uncertainties than the previous measurements [57,58]. Instead, we again applied a weighted least-squares fitting to all experimental data available in the literature for k_{24} [19,20,57,60–73] to yield a new rate correlation,

$$k_{24} = 10^{11.68\left(^{-4.86}_{+3.74}\right)} T^{0.66\left(^{+1.42}_{-1.15}\right)} \times \exp\left[-7485\begin{pmatrix}+2360\\-1380\end{pmatrix}\Big/ T\right] \text{cm}^3/\text{mol/s} \quad (3)$$

Figure 4 compares this new correlation with the literature data and the previous correlations. In the range of

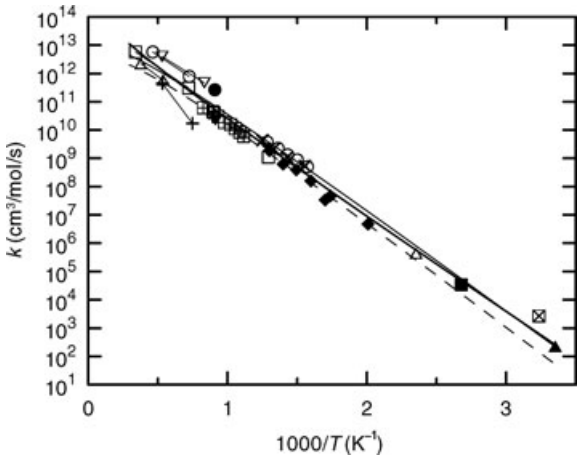

Figure 4 Rate constant of reaction $HCO + M \rightarrow H + CO + M$ (R24). Symbols and lines with symbols are literature results: ⊞ Friedrichs et al. [19]; —▽— Hidaka et al. [20]: ○ Timonen et al. [57]; ⊠ Pearson et al. [60]; —○— Schecker et al. [61]; —□— Browne et al. [62]; —+— Bowman [63]; ▲ Ahumada et al. [64]; □ Baldwin et al. [65]; ■ Wang et al. [66]; ▼ Westbrook et al. [67]; △ Campbell et al. [68]; ▽ Hochnadel et al [69]; ● Cherian et al. [70]; —△— Cribb et al. [71]; ◆ Krasnoperov et al. [72]; × Hippler et al. [73]. The dotted line is the recommendation of Timonen et al. [57], the dashed line is the recommendation of Friedrichs et al. [19], and the solid line represents the values used in the present model (Eq. (3)).

1500–2000 K, the prediction of Eq. (3) agrees with the data correlation of Timonen et al. [57] within 30% and is about 2–3 times higher than the correlation recommended by Friedrichs et al. [19]. Over 500–1300 K, where the rate coefficient of (R24) was measured by Friedrichs et al. [19], Timonen et al. [57], Krasnoperov et al. [72], and Hippler et al. [73], the current correlation predicts values almost equidistant from the measurements reported by Timonen et al. [57] and Friedrichs et al. [19].

It should be noted that the correlation shown in Eq. (3) was obtained by fitting low-pressure limit data. Timonen et al. [57] concluded, based on resonance theory, that significant deviations from the low-pressure limit would occur at (high) pressures beyond the scope of practical combustion processes, and reaction (R24) may be regarded as being in the low-pressure limit for most combustion applications. Recently, the pressure dependence of the rate constant of reaction (R24) has been measured by Krasnoperov et al. [72] and Hippler et al. [73], and the data show a somewhat unusual pressure falloff behavior. Based on their measurements and an isolated resonance model with variable resonance lifetimes, Hippler et al. [73] challenged the conclusions drawn by Timonen et al. [57] and indicated

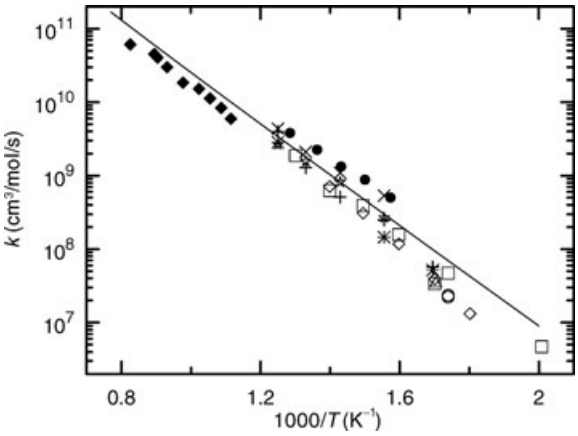

Figure 5 Pressure dependence of the rate constant of reaction (R24) as measured by Krasnoperov et al. [72] (□ : 1 bar; ◇ : 10 bar; △ : 30 bar; ○ : 100 bar) and Hippler et al. [73] (× : 1 bar; ☆ : 10 bar; ✳ : 30 bar; ✚ : 100 bar), the rate expression used in the present model (solid line) as well as the low pressure measurements of Friedrichs et al. [19] and Timonen et al. [57] (◆ and ●, respectively) are also shown for comparison.

that deviations from the low-pressure limit may occur even below atmospheric pressure; Krasnoperov [74], however, has questioned the experimental method and analyses performed by Hippler et al. [73] when obtaining low-pressure data (see [74,75] for full details). Figure 5 plots the pressure-dependent measurements of Krasnoperov et al. [72] and Hippler et al. [73] and compares them against the low-pressure data of Friedrichs et al. [19] and Timonen et al. [57] as well as Eq. (3). It is clearly seen that, even though falloff behavior is observed, the deviation from the low-pressure limit data is only significant at temperatures below 580 K; the calculated values (using Eq. (3)) are within a factor of 2–3 of the measured high-pressure data below this temperature. At lower temperatures and in any applications related to combustion, the reaction of HCO with HO_2 will be far more important than (R24). Therefore for combustion modeling, the use of a low-pressure limit rate constant for reaction (R24) causes no significant differences in model predictions. Regardless of this result, more studies of the falloff behavior of (R24) are warranted.

Because there are few specific experimental rate constant measurements at high temperatures for (R25) (e.g., see NIST kinetics database; http://kinetics.nist.gov), the recommendation of Timonen et al. [58] was retained [93]. Given the fact that the new rate expression for (R24) (Eq. (3)) does not deviate considerably from the recommendation of Timonen et al. [57] over the temperature range relevant to flow reactor studies, retaining this rate coefficient does not significantly alter the k_{24}/k_{25} ratio which, as mentioned above, is important for the CH_2O system at flow reactor conditions. More recently, Colberg and Friedrichs [76] published new measurements for the rate of reaction (R25) at both room temperature and in the temperature range of 739–1108 K. Implementing this newly proposed rate (k_{25} (295 K) $= 3.55 \times 10^{12}$; k_{25} (739–1108 K) $= 3.70 \times 10^{13} \exp(-1563/T)$ cm^3/mol/s) in the present mechanism has little impact on the quality of its predictions against targets discussed in the sections below. Under flow reactor conditions, this rate differs by no more than 20% from the recommendation of Timonen et al. [58], assuring a reasonable k_{24}/k_{25} ratio. At higher temperatures ($T > 1500$ K), however, the new rate correlation yields values approximately twice those recommended in [58] and results in some differences in the modeling of laminar flame speeds (see Fig. 1). Laminar flame speed predictions are changed by approximately 10%, slightly more than typical uncertainties in modern measurements reported in the literature. On the basis of these results and considering that the new expression of Colberg and Friedrichs [76] has not been validated at higher temperatures, we continue to use the recommendation of [58] in the model reported here.

CH_2O-Related Reactions

In addition to the modifications in specific rate constant correlations for reactions (R23), (R24), and (R25), other important reactions for the CH_2O/O_2 system were reviewed and the rate constants were updated to those appearing in more recent publications. These reactions include

$$CH_2O + M = H + HCO + M \quad \text{(R34)}$$

$$CH_2O + M = H_2 + CO + M \quad \text{(R35)}$$

$$CH_2O + H = HCO + H_2 \quad \text{(R36)}$$

$$CH_2O + HO_2 = HCO + H_2O_2 \quad \text{(R40)}$$

$$CH_2OH + HCO = CH_2O + CH_2O \quad \text{(R60)}$$

Formaldehyde oxidation is very sensitive to the abstraction reactions (R36) and (R40) under flow reactor conditions, and to the unimolecular decomposition reactions (R34) and (R35) in shock tube studies, as demonstrated earlier [9]. Eiteneer et al. [21] studied the ignition of CH_2O/O_2/Ar mixtures behind reflected shock waves and developed an expression for the rate constant of reaction (R40) by fitting their data and literature results. This new expression yields rates in close agreement with those used by Hochgreb and Dryer [9]

at intermediate temperatures (within 7% at 1000 K), while the predicted rate constant is about two times higher at 500 and 2000 K. In the current study, the rate correlation for (R40) suggested by Eiteneer et al. [21] was adopted.

Irdam et al. [77] performed formaldehyde pyrolysis experiments and transition state theory calculations for reaction (R36). The recommended rate coefficient, adopted in the present study, was later found to be in excellent agreement with the direct measurements of Friedrichs et al. [78]. In a shock tube study of CH_2O thermal decomposition, Friedrichs et al. [22] measured the species time history profiles of CH_2O and HCO and conducted RRKM calculations for reactions (R34) and (R35). The authors also presented a new value for the rate constant of reaction (R60), which becomes important for mixtures with high concentrations of CH_2O. The recommendations of Friedrichs et al. [22] for reactions (R34), (R35), and (R60) were used in the current mechanism. In addition, the rate coefficient of reaction,

$$CH_2OH + HCO = CH_3OH + CO \qquad (R59)$$

which competes with reaction (R60), was modified to 1×10^{13} cm^3/mol/s, thus keeping the branching ratio, k_{60}/k_{59}, the same as in the original mechanism [4].

Furthermore, in an effort to include in the present model the most up-to-date rate information for the systems treated in this study, the very recent measurements of the addition of OH and O_2 to formaldehyde (reactions (R38) and (R39), respectively) have been adopted from the studies of Vasudevan et al. [79,80]. The recommended rate constants [79,80] are within a factor of 2 of those suggested by Tsang and Hampson [81].

CH_3OH-Related Reactions

As in the case of formaldehyde, the methanol oxidation system is very sensitive to fuel abstraction and decomposition reactions [4]. There are several publications on the kinetics of these reactions that have appeared after the work of Held and Dryer [4]. In GRI-Mech 3.0 [47], the decomposition reactions of methanol were investigated using the RRKM theory and results were then fitted to several sets of experimental data published from 1984 to 1994. The obtained rate constants were expressed in Troe form [82] for the temperature and pressure dependence of the decomposition reactions. Koike et al. [83] have estimated the rate constant of the major decomposition reaction of methanol,

$$CH_3OH\ (+M) = CH_3 + OH\ (+M) \qquad (R72)$$

from shock tube experiments of CH_3OH pyrolysis at 0.4–0.82 atm and 1400–2500 K. Under these conditions, the estimated rate constant is in reasonable agreement (about 50%) with that provided in GRI-Mech 3.0. In a more recent study, Krasnoperov and Michael [84] have reported the experimental recombination rates of CH_3 and OH at conditions close to high-pressure limit that are lower than the high-pressure reverse rate of (R72) used by GRI-Mech. While detailed multichannel simulations of this system that would attempt to reconcile these new data are clearly warranted for future studies, the GRI-Mech 3.0 [47] rate constants for methanol decomposition reactions were adopted in the current study. There are two pathways for methanol abstraction reactions due to the two distinct sites of H atoms in CH_3OH molecules. Jimenez et al. [85] experimentally derived the total rate constants of the abstraction reaction

$$CH_3OH + OH \rightarrow \text{products}$$

at 235–360 K. The total rate constants agree within 20% with those of Bott and Cohen [86], which were used in the original mechanism [4] and retained in the present work.

RESULTS AND DISCUSSION

The revised C_1/O_2 mechanism as described above consists of 84 reversible elementary reactions among 18 species and the thermochemical data listed in Tables I and II, respectively. Reverse rate constants are computed from the forward rate constants and the equilibrium constants. The first 31 reactions listed in Table I can be used as the comprehensive kinetic model for CO combustion, and it predicts the same behavior of $CO/H_2/O_2$ systems as that found using the entire C_1 oxidation mechanism. The absence of potential C_2 submechanism elements as well as CH_2 (singlet and triplet states) reactions on CO, CH_2O, and CH_3OH oxidation predictions for the targets investigated here was tested by incorporating a C_2H_X (X = 1–6) reaction subset primarily taken from Wang et al. [112] and comparing predictions with the original mechanism. Negligible differences were found for all of the cases studied here. For example, the compiled C_2 mechanism predicts less than 1% higher CH_3OH/air flame speeds than the present C_1 model.

The current C_1/O_2 mechanism has been compared against a wide range of experimental results, including laminar flame speeds, shock tube ignition delay data, and species profiles measured in flow reactor, shock tube, and burner-stabilized flame studies. The

Table I Detailed C_1/O_2 Reaction Mechanism

#	Reaction		A	n	E_a	Reference
			H_2/O_2 reactions			
1	$H + O_2 = O + OH$		3.55E+15	−0.40	1.66E+04	[87]
2	$O + H_2 = H + OH$		5.08E+04	2.70	6.29E+03	[88]
3	$H_2 + OH = H_2O + H$		2.16E+08	1.50	3.43E+03	[89]
4	$O + H_2O = OH + OH$		2.97E+06	2.00	1.34E+04	[90]
5	$H_2 + M = H + H + M$		4.58E+19	−1.40	1.04E+05	[81]
	$\varepsilon_{H_2} = 2.5$, $\varepsilon_{H_2O} = 12.0$, $\varepsilon_{CO} = 1.9$, $\varepsilon_{CO_2} = 3.8$, $\varepsilon_{Ar} = 0.0$, $\varepsilon_{He} = 0.0$					
	$H_2 + Ar = H + H + Ar$		5.84E+18	−1.10	1.04E+05	[81]
	$H_2 + He = H + H + He$		5.84E+18	−1.10	1.04E+05	[81]
6	$O + O + M = O_2 + M$		6.16E+15	−0.50	0.00	[81]
	$\varepsilon_{H_2} = 2.5$, $\varepsilon_{H_2O} = 12.0$, $\varepsilon_{CO} = 1.9$, $\varepsilon_{CO_2} = 3.8$, $\varepsilon_{Ar} = 0.0$, $\varepsilon_{He} = 0.0$					
	$O + O + Ar = O_2 + Ar$		1.89E+13	0.00	−1.79E+03	[81]
	$O + O + He = O_2 + He$		1.89E+13	0.00	−1.79E+03	[81]
7	$O + H + M = OH + M$		4.71E+18	−1.00	0.00	[81]
	$\varepsilon_{H_2} = 2.5$, $\varepsilon_{H_2O} = 12.0$, $\varepsilon_{CO} = 1.9$, $\varepsilon_{CO_2} = 3.8$, $\varepsilon_{Ar} = 0.75$, $\varepsilon_{He} = 0.75$					
8	$H + OH + M = H_2O + M$		3.80E+22	−2.00	0.00	[18]
	$\varepsilon_{H_2} = 2.5$, $\varepsilon_{H_2O} = 12.0$, $\varepsilon_{CO} = 1.9$, $\varepsilon_{CO_2} = 3.8$, $\varepsilon_{Ar} = 0.38$, $\varepsilon_{He} = 0.38$					
9	$H + O_2 (+M) = HO_2 (+M)$	k_∞	1.48E+12	0.60	0.00	[91]
		k_0	6.37E+20	−1.72	5.25E+02	[71], M = N_2
	$\alpha = 0.8$, $T^{***} = 1.0E{-}30$, $T^* = 1.0E{+}30$					
	$\varepsilon_{H_2} = 2.0$, $\varepsilon_{H_2O} = 11.0$, $\varepsilon_{CO} = 1.9$, $\varepsilon_{CO_2} = 3.8$, $\varepsilon_{O2} = 0.78$					
	$H + O_2 (+M) = HO_2 (+M)$	k_∞	1.48E+12	0.60	0.00	[91]
		k_0	9.04E+19	−1.50	4.92E+02	[94], M = Ar or He
	$\alpha = 0.5$, $T^{***} = 1.0E{-}30$, $T^* = 1.0E{+}30$					
	$\varepsilon_{H_2} = 3.0$, $\varepsilon_{H_2O} = 16.0$, $\varepsilon_{CO} = 2.7$, $\varepsilon_{CO_2} = 5.4$, $\varepsilon_{O2} = 1.1$, $\varepsilon_{He} = 1.2$					
10	$HO_2 + H = H_2 + O_2$		1.66E+13	0.00	8.23E+02	[14]
11	$HO_2 + H = OH + OH$		7.08E+13	0.00	2.95E+02	[14]
12	$HO_2 + O = O_2 + OH$		3.25E+13	0.00	0.00	[95]
13	$HO_2 + OH = H_2O + O_2$		2.89E+13	0.00	−4.97E+02	[95]
14	$HO_2 + HO_2 = H_2O_2 + O_2$	Duplicate	4.20E+14	0.00	1.20E+04	[92]
	$HO_2 + HO_2 = H_2O_2 + O_2$	Duplicate	1.30E+11	0.00	−1.63E+03	
15	$H_2O_2 (+M) = OH + OH (+M)$	k_∞	2.95E+14	0.00	4.84E+04	[93]
		k_0	1.20E+17	0.00	4.55E+04	[41]
	$\alpha = 0.5$, $T^{***} = 1.0E{-}30$, $T^* = 1.0E{+}30$					
	$\varepsilon_{H_2} = 2.5$, $\varepsilon_{H_2O} = 12.0$, $\varepsilon_{CO} = 1.9$, $\varepsilon_{CO_2} = 3.8$, $\varepsilon_{Ar} = 0.64$, $\varepsilon_{He} = 0.64$					
16	$H_2O_2 + H = H_2O + OH$		2.41E+13	0.00	3.97E+03	[81]
17	$H_2O_2 + H = HO_2 + H_2$		4.82E+13	0.00	7.95E+03	[81]
18	$H_2O_2 + O = OH + HO_2$		9.55E+06	2.00	3.97E+03	[81]
19	$H_2O_2 + OH = HO_2 + H_2O$	Duplicate	1.00E+12	0.00	0.00	[96]
	$H_2O_2 + OH = HO_2 + H_2O$	Duplicate	5.80E+14	0.00	9.56E+03	
			CO reactions			
20	$CO + O (+M) = CO_2 (+M)$	k_∞	1.80E+10	0.00	2.38E+03	[97]
		k_0	1.55E+24	−2.79	4.19E+03	[98]
	$\varepsilon_{H_2} = 2.5$, $\varepsilon_{H_2O} = 12.0$, $\varepsilon_{CO} = 1.9$, $\varepsilon_{CO_2} = 3.8$, $\varepsilon_{Ar} = 0.87$					
21	$CO + O_2 = CO_2 + O$		2.53E+12	0.00	4.77E+04	[81]
22	$CO + HO_2 = CO_2 + OH$		3.01E+13	0.00	2.30E+04	[13]
23	$CO + OH = CO_2 + H$		2.23E+05	1.90	−1.16E+03	This study
			HCO reactions			
24	$HCO + M = H + CO + M$		4.75E+11	0.70	1.49E+04	This study
	$\varepsilon_{H_2} = 2.5$, $\varepsilon_{H_2O} = 6.0$, $\varepsilon_{CO} = 1.9$, $\varepsilon_{CO_2} = 3.8$					
25	$HCO + O_2 = CO + HO_2$		7.58E+12	0.00	4.10E+02	[58]
26	$HCO + H = CO + H_2$		7.23E+13	0.00	0.00	[57]
27	$HCO + O = CO + OH$		3.02E+13	0.00	0.00	[81]
28	$HCO + OH = CO + H_2O$		3.02E+13	0.00	0.00	[81]

Continued

Table I Continued

#	Reaction		A	n	E_a	Reference
29	$HCO + O = CO_2 + H$		3.00E+13	0.00	0.00	[81]
30	$HCO + HO_2 = CO_2 + OH + H$		3.00E+13	0.00	0.00	[81]
31	$HCO + HCO = H_2 + CO + CO$		3.00E+12	0.00	0.00	[81]
32	$HCO + CH_3 = CO + CH4$		1.20E+14	0.00	0.00	[81]
33	$HCO + HCO = CH_2O + CO$		3.00E+13	0.00	0.00	[59]
		CH_2O reactions				
34	$CH_2O + M = HCO + H + M$		3.30E+39	−6.30	9.99E+04	[22]
	$\varepsilon_{H_2} = 2.5$, $\varepsilon_{H_2O} = 12.0$, $\varepsilon_{CO} = 1.9$, $\varepsilon_{CO_2} = 3.8$, $\varepsilon_{Ar} = 0.87$					
35	$CH_2O + M = CO + H_2 + M$		3.10E+45	−8.00	9.75E+04	[22]
	$\varepsilon_{H_2} = 2.5$, $\varepsilon_{H_2O} = 12.0$, $\varepsilon_{CO} = 1.9$, $\varepsilon_{CO_2} = 3.8$, $\varepsilon_{Ar} = 0.87$					
36	$CH_2O + H = HCO + H_2$		5.74E+07	1.90	2.75E+03	[77]
37	$CH_2O + O = HCO + OH$		1.81E+13	0.00	3.08E+03	[81]
38	$CH_2O + OH = HCO + H_2O$		3.43E+09	1.20	−4.47E+02	[79]
39	$CH_2O + O_2 = HCO + HO_2$		1.23E+06	3.00	5.20E+04	[80]
40	$CH_2O + HO_2 = HCO + H_2O_2$		4.11E+04	2.50	1.02E+04	[21]
41	$CH_2O + CH_3 = HCO + CH_4$		3.64E−06	5.40	9.98E+02	[31]
		CH_3 reactions				
42	$CH_3 + O = CH_2O + H$		8.43E+13	0.00	0.00	[99]
43	$CH_3 + O_2 = CH_3O + O$		1.99E+18	−1.60	2.92E+04	[81]
44	$CH_3 + O_2 = CH_2O + OH$		3.74E+11	0.00	1.46E+04	[100]
45	$CH_3 + HO_2 = CH_3O + OH$		2.41E+10	0.80	−2.33E+03	[26]
46	$CH_3 + H\ (+M) = CH_4\ (+M)$	k_∞	1.27E+16	−0.60	3.83E+02	[101]
		k_0	2.48E+33	−4.76	2.44E+03	[101]
	$\alpha = 0.783$, $T^{***} = 7.40E+01$, $T^* = 2.94E+03$, $T^{**} = 6.96E+03$					
	$\varepsilon_{H_2} = 2.0$, $\varepsilon_{H_2O} = 6.0$, $\varepsilon_{CO} = 1.5$, $\varepsilon_{CO_2} = 2.0$, $\varepsilon_{Ar} = 0.7$, $\varepsilon_{CH_4} = 2.0$					
		CH_4 reactions				
47	$CH_4 + H = CH_3 + H_2$		5.47E+07	2.00	1.12E+04	[102]
48	$CH_4 + O = CH_3 + OH$		3.15E+12	0.50	1.03E+04	[103]
49	$CH_4 + OH = CH_3 + H_2O$		5.72E+06	2.00	2.64E+03	[104]
50	$CH_3 + HO_2 = CH_4 + O_2$		3.16E+12	0.00	0.00	[100]
51	$CH_4 + HO_2 = CH_3 + H_2O_2$		1.81E+11	0.00	1.86E+04	[81]
		CH_2OH reactions				
52	$CH_2OH + M = CH_2O + H + M$		1.00E+14	0.00	2.51E+04	[71]
53	$CH_2OH + H = CH_2O + H_2$		6.00E+12	0.00	0.00	[105]
54	$CH_2OH + H = CH_3 + OH$		9.64E+13	0.00	0.00	[81]
55	$CH_2OH + O = CH_2O + OH$		4.20E+13	0.00	0.00	[105]
56	$CH_2OH + OH = CH_2O + H_2O$		2.40E+13	0.00	0.00	[105]
57	$CH_2OH + O_2 = CH_2O + HO_2$	Duplicate	2.41E+14	0.00	5.02E+03	[106]
	$CH_2OH + O_2 = CH_2O + HO_2$	Duplicate	1.51E+15	−1.00	0.00	
58	$CH_2OH + HO_2 = CH_2O + H_2O_2$		1.20E+13	0.00	0.00	[105]
59	$CH_2OH + HCO = CH_3OH + CO$		1.00E+13	0.00	0.00	See text
60	$CH_2OH + HCO = CH_2O + CH_2O$		1.50E+13	0.00	0.00	[22]
61	$2CH_2OH = CH_3OH + CH_2O$		3.00E+12	0.00	0.00	[105]
62	$CH_2OH + CH_3O = CH_3OH + CH_2O$		2.40E+13	0.00	0.00	[105]
		CH_3O reactions				
63	$CH_3O + M = CH_2O + H + M$		8.30E+17	−1.20	1.55E+04	[107]
64	$CH_3O + H = CH_3 + OH$		3.20E+13	0.00	0.00	[108]
65	$CH_3O + O = CH_2O + OH$		6.00E+12	0.00	0.00	[81]
66	$CH_3O + OH = CH_2O + H_2O$		1.80E+13	0.00	0.00	[81]
67	$CH_3O + O2 = CH_2O + HO_2$	Duplicate	9.03E+13	0.00	1.20E+04	[108]
	$CH_3O + O2 = CH_2O + HO_2$	Duplicate	2.20E+10	0.00	1.75E+03	
68	$CH_3O + HO_2 = CH_2O + H_2O_2$		3.00E+11	0.00	0.00	[81]

Continued

Table I Continued

#	Reaction		A	n	E_a	Reference
69	$CH_3O + CO = CH_3 + CO_2$		1.60E+13	0.00	1.18E+04	[81]
70	$CH_3O + HCO = CH_3OH + CO$		9.00E+13	0.00	0.00	[81]
71	$2CH_3O = CH_3OH + CH_2O$		6.00E+13	0.00	0.00	[81]
		CH_3OH reactions				
72	$OH + CH_3$ (+M) $= CH_3OH$ (+M)	k_∞	2.79E+18	−1.40	1.33E+03	[47]
		k_0	4.00E+36	−5.92	3.14E+03	[47]
	$\alpha = 0.412$, $T^{***} = 1.95$E+02, $T^* = 5.90$E+03, $T^{**} = 6.39$E+03					
	$\varepsilon_{H_2} = 2.0$, $\varepsilon_{H_2O} = 6.0$, $\varepsilon_{CO} = 1.5$, $\varepsilon_{CO_2} = 2.0$, $\varepsilon_{CH_4} = 2.0$					
73	$H + CH_2OH$ (+ M) $= CH_3OH$ (+ M)	k_∞	1.06E+12	0.50	8.60E+01	[47]
		k_0	4.36E+31	−4.65	5.08E+03	[47]
	$\alpha = 0.6$, $T^{***} = 1.00$E+02, $T^* = 9.00$E+04, $T^{**} = 1.00$E+04					
	$\varepsilon_{H_2} = 2.0$, $\varepsilon_{H_2O} = 6.0$, $\varepsilon_{CO} = 1.5$, $\varepsilon_{CO_2} = 2.0$, $\varepsilon_{CH_4} = 2.0$,					
74	$H + CH_3O$ (+M) $= CH_3OH$ (+M)	k_∞	2.43E+12	0.50	5.00E+01	[47]
		k_0	4.66E+41	−7.44	1.41E+04	[47]
	$\alpha = 0.7$, $T^{***} = 1.00$E+02, $T^* = 9.00$E+04, $T^{**} = 1.00$E+04					
	$\varepsilon_{H_2} = 2.0$, $\varepsilon_{H_2O} = 6.0$, $\varepsilon_{CO} = 1.5$, $\varepsilon_{CO_2} = 2.0$, $\varepsilon_{CH_4} = 2.0$					
75	$CH_3OH + H = CH_2OH + H_2$		3.20E+13	0.00	6.10E+03	[41]
76	$CH_3OH + H = CH_3O + H_2$		8.00E+12	0.00	6.10E+03	[41]
77	$CH_3OH + O = CH_2OH + OH$		3.88E+05	2.50	3.08E+03	[105]
78	$CH_3OH + OH = CH_3O + H_2O$		1.00E+06	2.10	4.97E+02	[86]
79	$CH_3OH + OH = CH_2OH + H_2O$		7.10E+06	1.80	−5.96E+02	[86]
80	$CH_3OH + O_2 = CH_2OH + HO_2$		2.05E+13	0.00	4.49E+04	[105]
81	$CH_3OH + HCO = CH_2OH + CH_2O$		9.64E+03	2.90	1.31E+04	[105]
82	$CH_3OH + HO_2 = CH_2OH + H_2O_2$		3.98E+13	0.00	1.94E+04	[109]
83	$CH_3OH + CH_3 = CH_2OH + CH_4$		3.19E+01	3.20	7.17E+03	[105]
84	$CH_3O + CH_3OH = CH_3OH + CH_2OH$		3.00E+11	0.00	4.06E+03	[105]

Units are cm^3 mol s cal K; $k = AT^n \exp(-E_a/RT)$.

Table II Thermochemical Data for Species Considered in the C_1/O_2 Mechanism

Species	$\Delta H_{f(298)}$	$S_{(298)}$	$C_{P\,300\ K}$	$C_{P\,500\ K}$	$C_{P\,800\ K}$	$C_{P\,1000\ K}$	$C_{P\,1500\ K}$	$C_{P\,2000\ K}$	Reference
Ar	0	36.98	4.97	4.97	4.97	4.97	4.97	4.97	[110]
CH_2O	−27.71	52.33	8.41	10.48	13.36	14.91	16.92	18.08	[110]
CH_2OH	−4.25	58.36	11.36	14.19	17.07	18.42	20.65	21.86	See text
CH_3	35.06	46.37	9.2	10.75	12.86	14.09	16.25	17.57	[111]
CH_3O	3.9	54.61	9.08	12.43	16.63	18.6	21.51	23.26	[110]
CH_3OH	−48.06	57.28	10.51	14.26	19.08	21.4	25.02	27.25	[110]
CH_4	−17.9	44.47	8.43	11.14	15	17.25	20.63	22.59	[110]
CO	−26.42	47.22	6.95	7.14	7.61	7.95	8.41	8.67	[110]
CO_2	−94.06	51.08	8.91	10.65	12.32	12.99	13.93	14.44	[110]
H	52.1	27.39	4.97	4.97	4.97	4.97	4.97	4.97	[110]
H_2	0	31.21	6.9	7	7.07	7.21	7.73	8.18	[110]
H_2O	−57.8	45.1	8	8.45	9.22	9.87	11.26	12.22	[110]
H_2O_2	−32.53	55.66	10.42	12.35	14.29	15.21	16.85	17.88	[110]
HCO	10.4	53.66	8.25	9.28	10.74	11.52	12.56	13.14	[110]
He	0	30.12	4.97	4.97	4.97	4.97	4.97	4.97	[110]
HO_2	3	54.76	8.35	9.47	10.77	11.38	12.48	13.32	See text
N_2	0	45.77	6.95	7.08	7.5	7.83	8.32	8.6	[110]
O	59.56	38.47	5.23	5.08	5.02	5	4.98	4.98	[110]
O_2	0	49.01	7.01	7.44	8.07	8.35	8.72	9.03	[110]
OH	8.9	43.91	7.16	7.05	7.15	7.34	7.87	8.28	See text

Units are cal/mol/K for $S_{(298)}$ and C_P, and kcal/mol for $\Delta H_{f(298)}$.

Table III Literature Experiments Used for Validation of CO/O_2 Mechanism

Method	Source	Mixture	T(K)	P(atm)	ϕ
Shock tube	Gardiner et al. [117]	$CO/H_2/O_2/Ar$	1400–2500	0.15–0.3	0.4
	Dean et al. [116]	$CO/H_2/O_2/Ar$	2000–2850	1.2–2.2	1.6–6.1
Laminar premixed flame	McLean et al. [48]	CO/H_2/air	298	1	0.5–6.0
	Huang et al. [23]	$CO/H_2/N_2$/air	298	1	0.7–1.4
Flow reactor	Yetter et al. [8]	$CO/H_2O/O_2/N_2$	1033	1	0.44–1.44
	Kim et al. [10]	$CO/H_2O/O_2/N_2$	960–1200	1.0–9.6	0.33–2.1
	Mueller et al. [118]	CO/H_2O /O_2/N_2	1038	1.0–9.6	1.0

Table IV Literature Experiments Used for Validation of CH_2O/O_2 Mechanism

Method	Source	Mixture	T(K)	P(atm)	ϕ
Shock tube	Dean et al. [132]	$CH_2O/O_2/Ar$	1935–2150	1.1–1.3	Pyrolysis, 0.67
	Buxton and Simpson [126]	CH_2O/Ar	1750–2100	0.6–3.5	Pyrolysis
	Hidaka et al. [20]	$CH_2O/O_2/Ar$	1240–1950	1.5–2.9	Pyrolysis, 4.0
	Eiteneer et al. [21]	$CH_2O/O_2/Ar$	1440–2120	0.9–2.3	Pyrolysis, 6.0
	Friedrichs et al. [19]	CH_2O/Ar	955–975	0.3–1.8	Pyrolysis
Burner-stabilized flame	Vandooren et al. [127]	CH_2O/O_2	300	0.03	0.22
Flow reactor	Hochgreb and Dryer [9]	CH_2O /O_2/N_2	945–1095	1	0.013–1.74
	This study	CH_2O /$H_2O/O_2/N_2$	850–950	1.5–6.0	~0.005

SENKIN code [113] was used to simulate experimental conditions in shock tubes and flow reactors assuming adiabatic systems under constant volume and constant pressure, respectively. The PREMIX code [114] was used for flame calculations. We used the standard CHEMKIN transport package [115] with Soret effects and multicomponent diffusion included. To assure a fully converged flame speed prediction, a minimum of 1000 grid points was imposed in the PREMIX calculations. Tables III–V list the experiments that the current $CO/H_2/O_2$, CH_2O/O_2, and CH_3OH/O_2 mechanism has been compared against. Representative results for these comparisons are shown in Figs. 6–26. The performance of each of the hierarchical submechanisms involving carbon is discussed below.

$CO/H_2/O_2$ Mechanism Predictions

Comparisons in Figs. 6 and 7 show that the predictions of the current CO oxidation mechanism are in good agreement with the premixed laminar flame speed measurements for $CO/H_2/O_2/N_2$ mixtures at atmospheric pressure. Predictions also compare very well with shock tube ignition delay data, as demonstrated in Figs. 8 and 9. The predicted ignition delay times presented in these figures were defined as the time required for CO_2 [116] or OH [117] concentration to reach a specified value, similar to the criteria used in the experimental work. Figures 10 and 11 show the time history of major species under flow reactor conditions. Predictions using the current mechanism agree very well with all of the experimental target information.

Sensitivity analyses were performed based on the present CO oxidation mechanism for three representative cases: the laminar premixed flame speed at equivalence ratio of 5.0 [48], the mass fraction of CO in a VPFR case at 3.5 atm [118], and the ignition delay time under the shock tube conditions of Dean et al. [116]. The most sensitive reactions along with their sensitivity coefficients are shown in Fig. 12. The normalized sensitivity coefficient of a reaction is defined as, $\partial \ln Y/\partial \ln k$, $\partial \ln s/\partial \ln k$, and $\partial \ln \tau/\partial \ln k$ for the disappearance of a species Y in a flow reactor, for laminar flame speed, and for ignition delay time,

Table V Literature Experiments Used for Validation of CH_3OH/O_2 Mechanism

Method	Source	Mixture	T(K)	P(atm)	ϕ
Shock tube	Bowman [130]	CH_3OH/O_2/CO/Ar	1545–2180	1.2–4.7	0.375–6.0
Laminar premixed flame	Egolfopoulos et al. [131]	CH_3OH/air	318–368	1.0	0.5–2.0
Flow reactor	Aronowitz et al. [128]	$CH_3OH/O_2/N_2$	1000–1010	1.0	0.05–1.6
	Norton and Dryer [129]	$CH_3OH/O_2/N_2$	1027–1034	1.0	0.6–1.6
	Held [28]	$CH_3OH/O_2/N_2$	750–1040	1.5–20.0	0.3–2.6

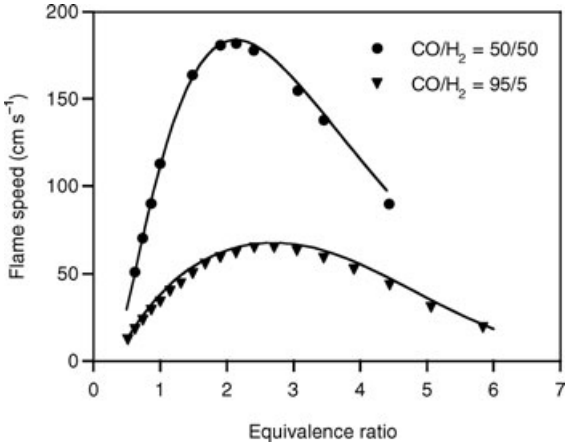

Figure 6 Laminar flame speeds of CO/H_2/air mixtures at 298 K and 1 atm for two fuel compositions (95% CO + 5% H_2 or 50% CO + 50% H_2). Symbols represent the experimental data [48], and lines are predictions of the present $CO/H_2/O_2$ mechanism.

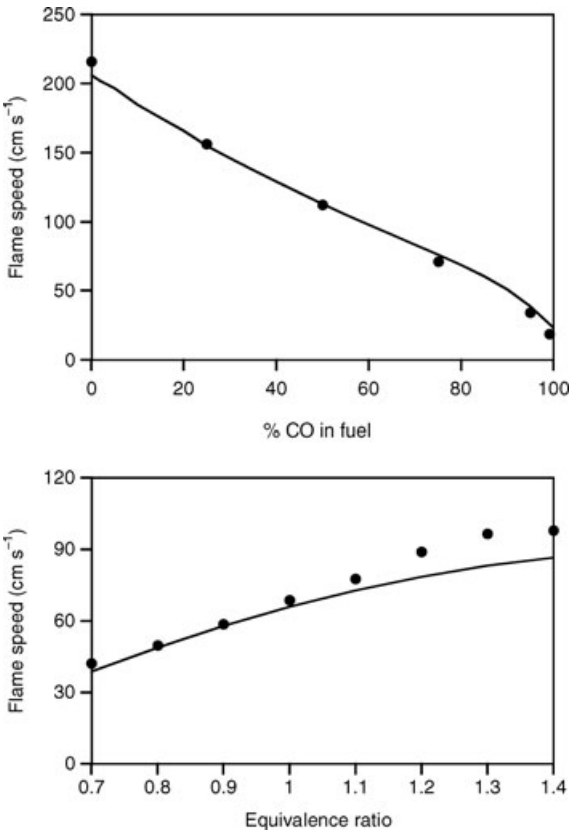

Figure 7 Laminar flame speeds for stoichiometric CO/H_2/air mixtures (top) and reformer gas/air mixtures (bottom) at 298 K and 1 atm. Composition of reformer gas is 28% H_2, 25% CO, and 47% N_2. Symbols represent the experimental data of McLean et al. [48] (top), and Huang et al. [23] (bottom). Lines are predictions of the present $CO/H_2/O_2$ mechanism.

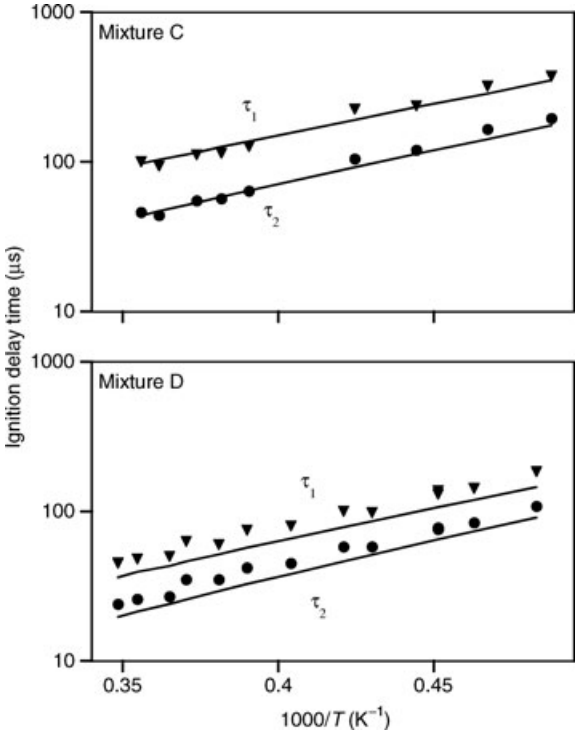

Figure 8 Ignition delay times of $CO/H_2/O_2$/Ar mixtures. The composition of mixture C is 0.049% H_2, 1.01% O_2, 3.28% CO, and balance Ar. The composition of mixture D is 0.05% H_2, 1.00% O_2, 12.17% CO, and balance Ar. Ignition delay time τ_1 is defined as the time when $[CO_2]$ reaches 2.4×10^{16} molecule/cm^3 for mixture C and 3.0×10^{16} molecule/cm^3 for mixture D. Time τ_2 is defined as the time when $[CO_2]$ reaches 8.0×10^{15} molecule/cm^3 for mixture C and 1.0×10^{16} molecule/cm^3 for mixture D. Symbols represent the experimental data [116], and lines are predictions of the present $CO/H_2/O_2$ mechanism.

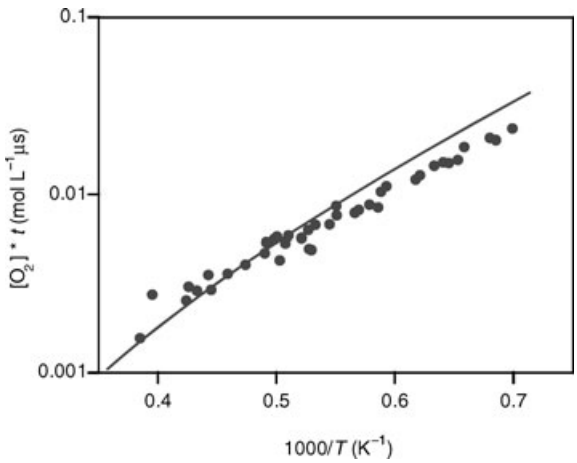

Figure 9 Induction times of $CO/H_2/O_2$/Ar mixtures in a shock tube. Initial condition: CO = 3.0%, H_2 = 1.0%, O_2 = 5.0% with balance Ar at 0.15–0.3 atm. Symbols represent the experimental data of Gardiner et al. [117], and the solid line shows predictions of the present $CO/H_2/O_2$ mechanism.

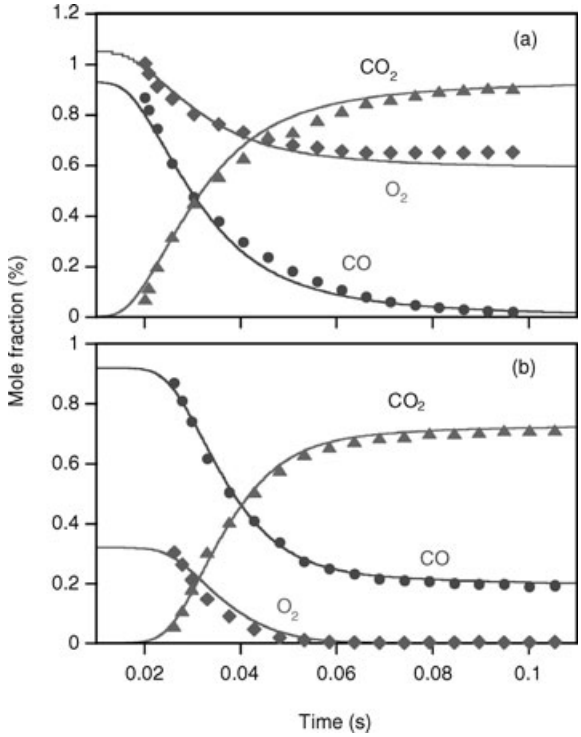

Figure 10 Reaction profiles of $CO/H_2O/O_2/N_2$ mixtures in an atmospheric pressure flow reactor. Initial condition: (a) $CO = 0.93\%$, $H_2O = 0.58\%$, $O_2 = 1.05\%$ with balance N_2 at 1033 K; (b) $CO = 0.92\%$, $H_2O = 0.59\%$, $O_2 = 0.32\%$ with balance N_2 at 1034 K. Symbols represent the experimental data of Yetter et al. [8], and lines are predictions of the present $CO/H_2/O_2$ mechanism. Model predictions are time shifted to match the 50% fuel consumption point.

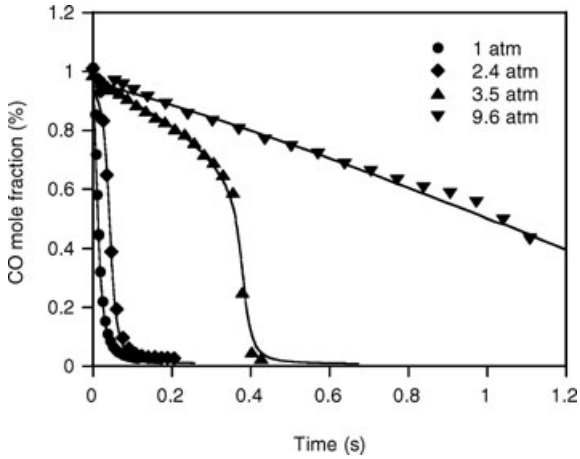

Figure 11 Reaction profiles of $CO/H_2O/O_2/N_2$ mixtures in a variable pressure flow reactor. Initial condition: $CO = 1.01\%$, $H_2O = 0.65\%$, $O_2 = 0.52\%$ with balance N_2 at 1038 K and 1.0 atm; $CO = 1.01\%$, $H_2O = 0.65\%$, $O_2 = 0.50\%$ with balance N_2 at 1038 K and 2.4 atm; $CO = 0.99\%$, $H_2O = 0.65\%$, $O_2 = 0.49\%$ with balance N_2 at 1038 K and 3.5 atm; $CO = 0.99\%$, $H_2O = 0.65\%$, $O_2 = 0.49\%$ with balance N_2 at 1040 K and 9.6 atm. Symbols represent the experimental data of Mueller et al. [16], and lines are predictions of the present $CO/H_2/O_2$ mechanism. Model predictions are time shifted to match the 50% fuel consumption point.

respectively, where k is the rate constant of the reaction, Y the mass fraction of a species, s the laminar flame speed, and τ the ignition delay time. In addition to those reactions within the H_2/O_2 submechanism (which govern the radical pool), $CO/H_2/O_2$ combustion is most sensitive to the chain propagation reaction (R23) and to the chain termination reaction,

$$CO + O\ (+M) = CO_2\ (+M) \qquad \text{(R20)}$$

The potential use of mixtures of hydrogen and carbon monoxide (syngas) in combined cycle gas turbine combustion at high pressures is stimulating new interest in the behavior of these submechanisms at high pressures. Very recently, new experiments involving carbon monoxide and carbon monoxide–hydrogen mixtures in rapid compression machines (RCM) [119] and high-pressure shock tubes [120] have begun to appear that represent targets significantly beyond the parameter ranges of previously available validation data sources. Mittal et al [119] used an early release of the present mechanism and reported discrepancies between simulations and their RCM ignition results and attributed these to the importance of HO_2/H_2O_2 chemistry under high pressures.

In light of these results and in order to further clarify the relative importance of specific elementary reactions on the chemical kinetic ignition of $CO/H_2/O_2/N_2$ mixtures at high pressure, we applied a computational singular perturbation (CSP) analysis approach we have recently demonstrated [121] as well as elementary sensitivity analyses. Unlike prior implementations of CSP methodology, the present formulation includes temperature as one of the state variables so that factors controlling ignition can be unambiguously determined. As developed [121], the methodology is applicable to the analysis of systems that can be modeled as constant volume processes (e.g., shock tubes). However, given recent experimental RCM data [119], the initially developed technique was further modified to accommodate systems with volume changes as a function of time. Incorporating a volume change as a function of time is the method used by Sung and coworkers [119, 122] to account for nonadiabatic compression in RCM experiments. The importance of individual reactions within the CSP methodology used here is described in terms of participation index (see [121] for details).

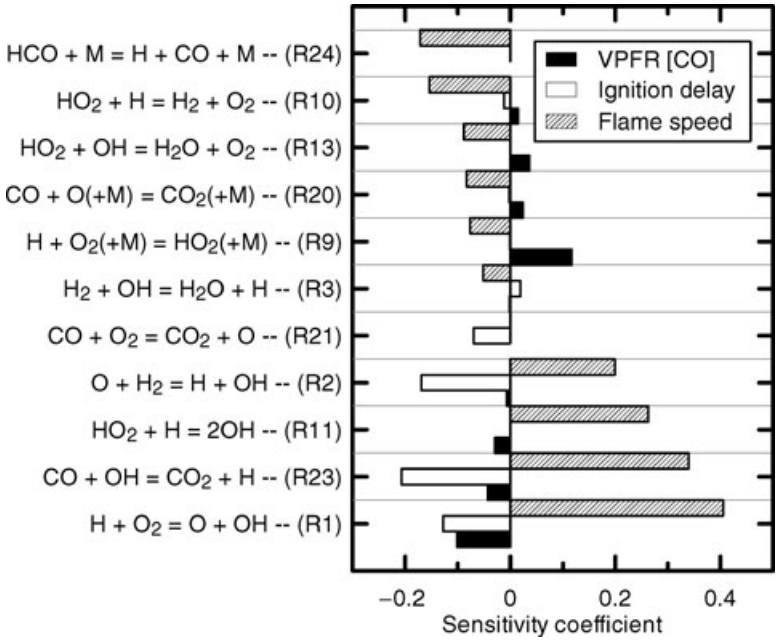

Figure 12 Sensitivity coefficients of reactions for flow reactor [16], laminar premixed flame [48], and shock tube [116] cases. Initial conditions: 0.99% CO, 0.49% O_2, 0.65% H_2O with balance N_2 at 3.5 atm and 1038 K [16]; 3.28% CO, 1.01% O_2, 0.049% H_2 with balance Ar at 1.41 atm and 2250 K [116]; 64.3% CO, 6.8% O_2, 3.4% H_2 with balance N_2 at 1.0 atm and 298 K [48]. The sensitivity coefficient for the flow reactor case is taken at the time when 50% CO has been consumed. The shock tube ignition delay time is defined as the time when CO_2 concentration reaches 8×10^{15} molecule/cm^3.

Figure 13 shows the relative importance of reactions most significantly affecting the heat release rate (reaction temperature) under the RCM conditions of Mittal et al. [119] at specific reaction times after the end of the compression stroke. What is clearly apparent is that the reactions $CO + O + M = CO_2 + M$ (R20) and $CO + HO_2 = CO_2 + OH$ (R22) are important only during the chemical induction period. After chemical ignition occurs, these reactions no longer contribute significantly to the rate of heat release. On the other hand, reactions such as $HO_2 + OH = H_2O + O_2$ (R13), $HO_2 + H = 2OH$ (R11), $H_2 + OH = H_2O + H$ (R3), and $H_2 + O = H + OH$ (R2) are significant in describing the heat release rate. A sensitivity analysis, which separately considers the sensitivity of the extent of reaction to the various reactions prior to and after ignition occurs, confirms the above findings for the importance of reactions (R20) and (R22). This indicates that HO_2 and H_2O_2 chemistry becomes important under the RCM conditions considered here, consistent with the conclusions of Mittal et al. [119], as these intermediate species rapidly build up during the induction period, more so than H or OH. Once ignition occurs, OH reactions become more dominant as evidenced by Fig. 13 (e.g., $CO + OH$ (R23) becomes one of the primary reactions at ignition as opposed to $CO + HO_2$ (R22) during the induction period).

Sivaramakrishnan et al. [120] have also studied H_2/CO oxidation in a shock tube at much higher pressures (exceeding 200 atm) and somewhat higher temperatures (>1100 K) for highly dilute H_2/CO/O_2/Ar mixtures. CSP analysis was applied to a representative case, as shown in Fig. 14. Figure 14b shows that under these high-pressure and high-temperature conditions, and for the highly dilute mixtures studied, there is not a well-defined ignition delay in the pressure history. There is, however, an obvious induction period. Similar to the RCM analysis above, CSP was performed during this induction period and the results are shown in Fig. 14c. The identified reactions participating in the evolution of the system are essentially different from those shown in Fig. 13 for the RCM case. It is important to note from Fig. 14c that reaction (R22), even though present in the initial evolution stages, quickly loses importance, more so than in the case shown in Fig. 13 with reaction (R13) becoming much more dominant as the system evolves. Therefore, the present CSP analysis shows that for highly dilute mixtures at sufficiently high pressures and temperatures, reaction (R13) needs to be considered in order to properly describe the H_2/CO kinetic system, whereas under more moderate pressures and reaction

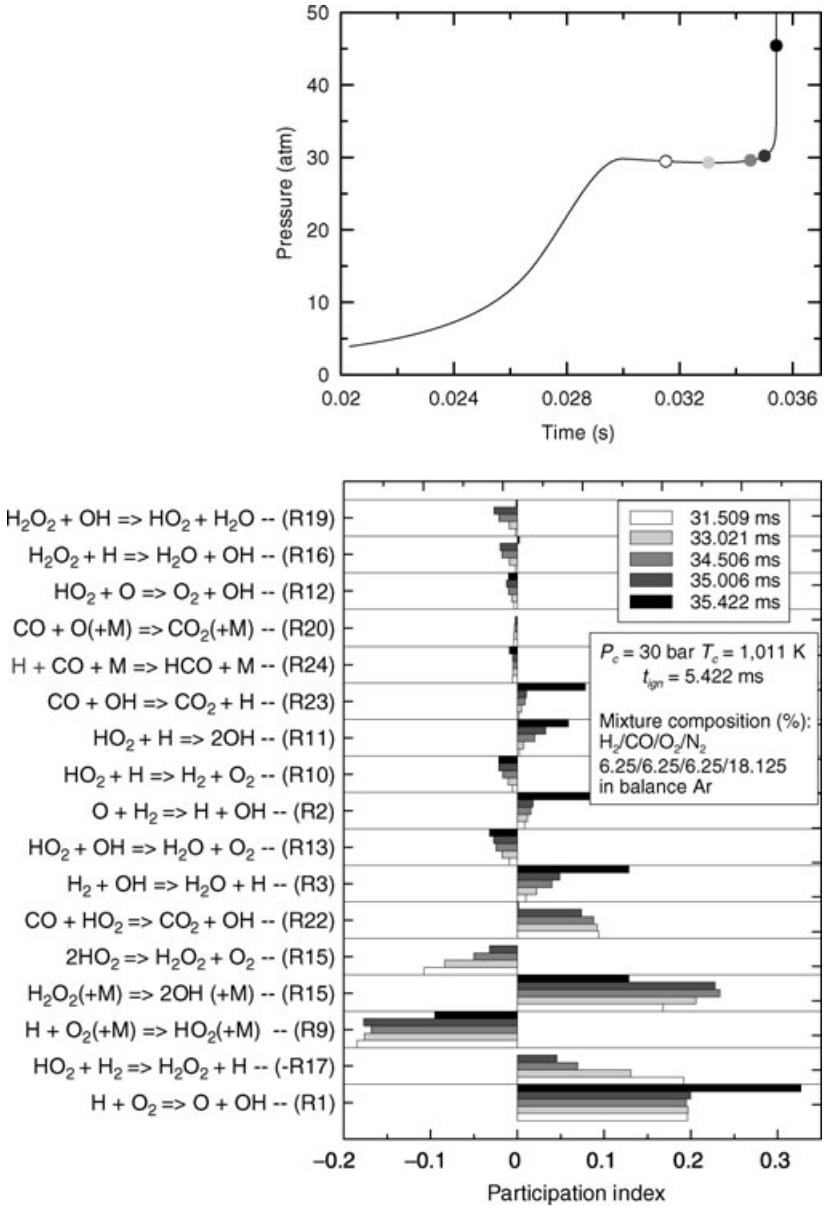

Figure 13 Reactions participating in the thermal evolution of a $H_2/CO/N_2/Ar$ kinetic system under rapid compression machine conditions (Mittal et al. [119]) obtained from CSP analysis. Analyses were performed after the compression stroke at the selected points shown in the top figure.

temperatures (R22) needs to be taken into account in predictions in which chemical induction processes are expected to be important. It is further noted that a similar analysis under the pressure/temperature conditions shown in Fig. 14 using higher reactant concentrations (as those shown in Fig. 13) identifies the same relative importance of reactions shown in Fig. 13; dilution, thus, plays a role in the relative importance of specific reactions for these different investigations.

Figures 13 and 14 show that reactions (R13) and (R22) appear to have, separately, a distinct impact on these systems. At pressures and temperatures similar to those in the work of Sivaramakrishnan et al. [120], the current C_1 model predictions are unchanged by a variation of as much as a factor of 5 in the rate of reaction (R22). In contrast, changes in reaction (R13) yield little effect in the RCM modeling. Reaction (R22) has been shown to have a strong sensitivity in the RCM studies [119], and as shown here it is expected to have little effect on any observable other than the chemical induction time. Reactions (R13) and (R22) are the subject of new studies that have recently appeared in the literature

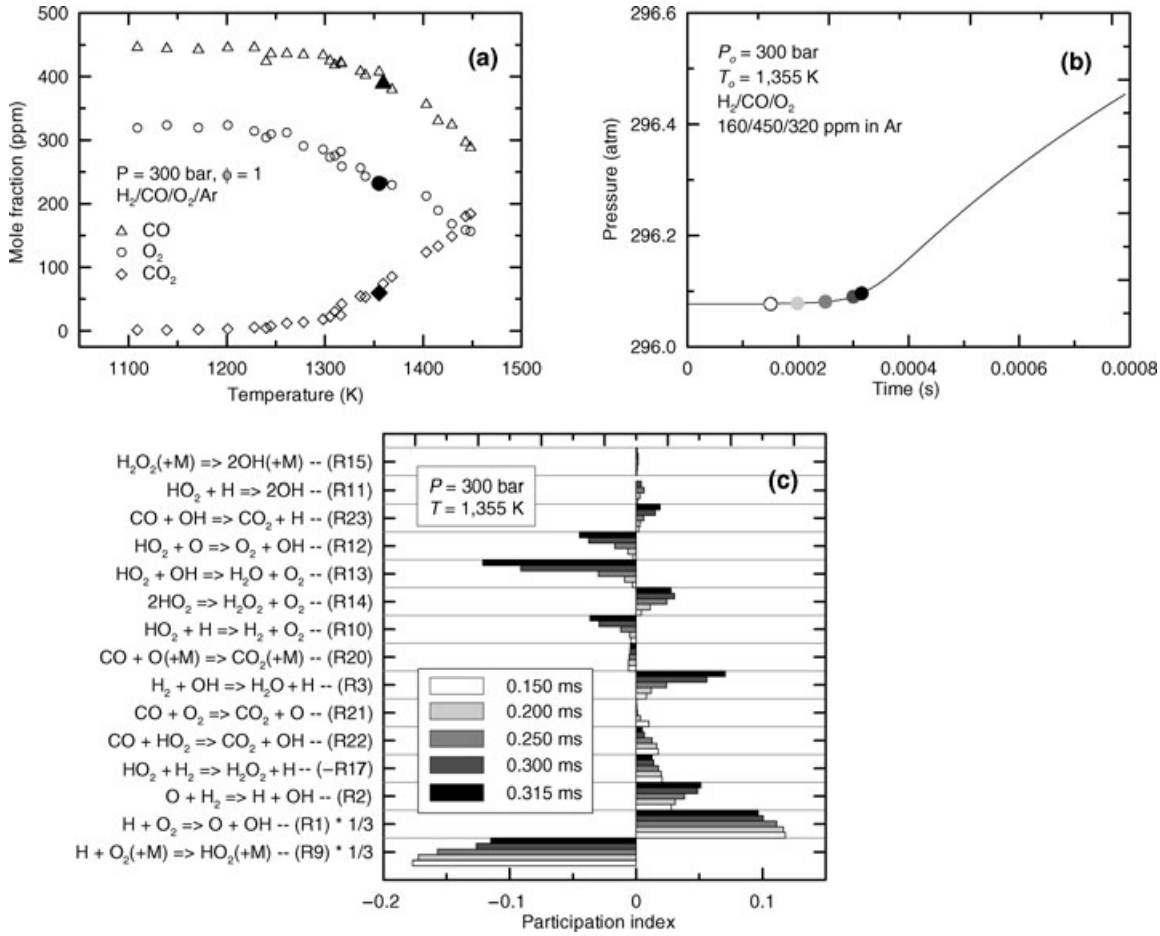

Figure 14 H_2/CO oxidation in a high-pressure shock tube. (a) Experimental data of Sivaramakrishnan et al. [120]; (b) temperature profile and (c) CSP analysis during the induction period in (b) for the conditions chosen in (a) (filled symbols). Note that the participation indices of reactions (R1) and (R9) have been reduced by one third to better display the spectrum of other reactions involved in the system.

[123,124] and which suggest [124] a much lower rate for (R22) than that presently employed. Implementing the recommendations for (R13) [123] and (R22) [124] in the present model yields very good agreement with data presented in those studies. Large uncertainties still exist, however, in both reactions (R13) and (R22) (e.g., see the work of Kappel et al. [125] for the highly nonlinear behavior of (R13)). Therefore, we acknowledge that further insights into elementary HO_2/H_2O_2 kinetics (and, especially, investigations of the rates of (R13) and (R22)) are warranted to properly model experimental data in these high-pressure venues [119,120,123,124] using the present mechanism. We have retained the current rate expressions for these reactions because the present mechanism performs satisfactorily under a wide pressure and temperature range for a variety of fuel systems. Finally, it should be noted that the very high participation index of $H + O_2 + M = HO_2 + M$ (R9) (see Figs. 13 and 14) results in a significant influence of third body effects on both induction and postinduction kinetics.

CH_2O/O_2 Mechanism

Comparisons of the current CH_2O/O_2 mechanism with representative formaldehyde experiments are shown in Figs. 15–20. Formaldehyde readily polymerizes at ambient conditions. In the experiments, pure formaldehyde was generated by heating either paraformaldehyde [20] or trioxane [21] to more than 100°C. Figure 15 shows the comparison of predictions with formaldehyde pyrolysis and oxidation measurements in a shock tube [21], including the time when CO concentration reaches 0.25 and 0.5 times its maximum value (Figs. 15a and 15b), and the profiles of CO concentration normalized by its maximum (Figs. 15c and 15d). The

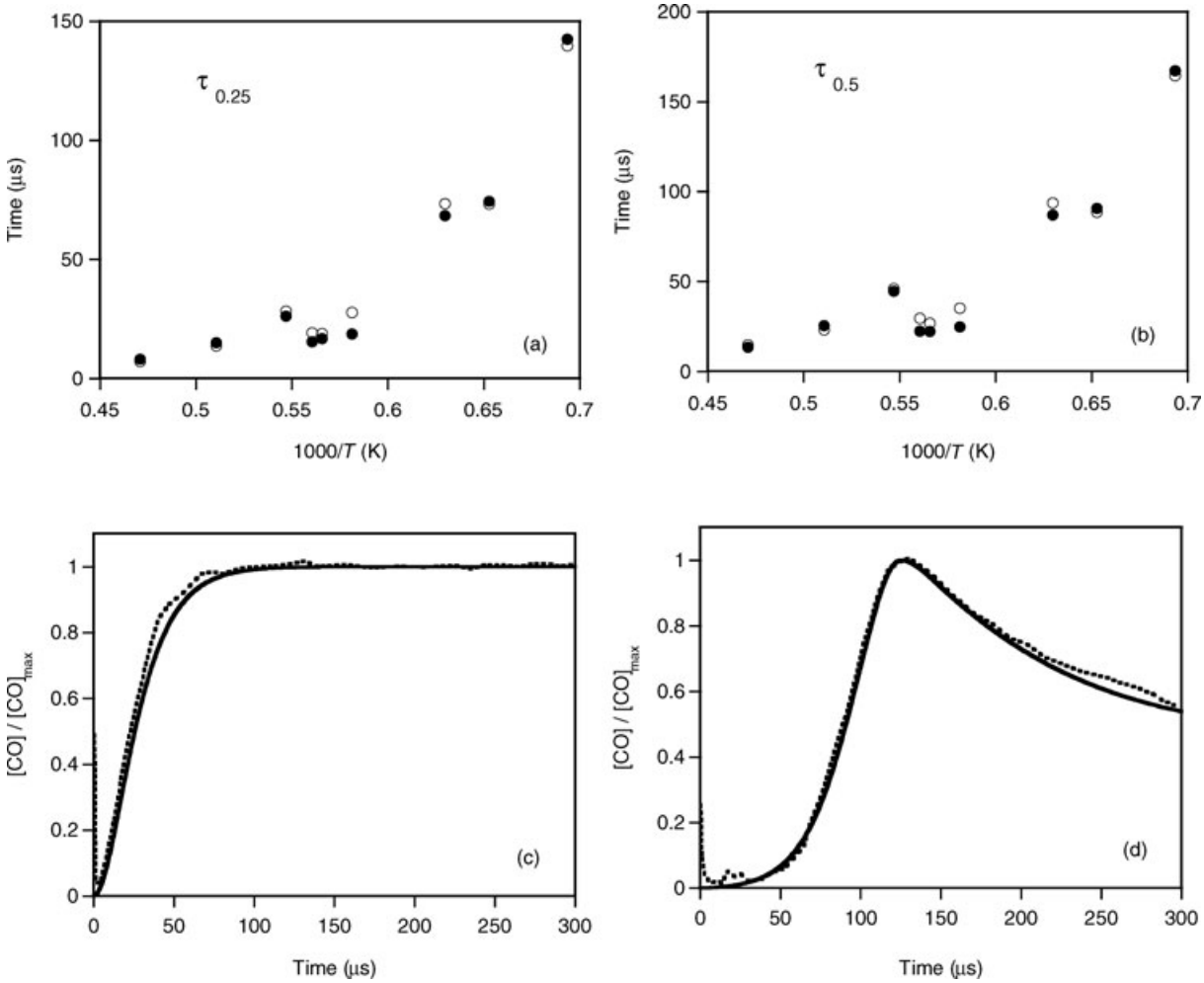

Figure 15 Ignition delay results for CH_2O/O_2/Ar mixture in a shock tube. In (a) and (b), initial conditions are for cases 10, 14, 24, 33, 47, 62, 70, 74, and 98 listed in Table 1 of Eiteneer et al. [21]. Initial conditions for (c) are 1.97% CH_2O with balance Ar at 1959 K and 1. 27 atm; for (d) 1.5% CH_2O, 1.5% O_2 with balance Ar at 1532 K and 1.35 atm. $\tau_{0.25}$ and $\tau_{0.5}$ are the time when the CO concentration reaches 0.25 and 0.5 times its maximum value, respectively. Open symbols and dashed lines represent experimental data [21], solid symbols and solid lines represent predictions of the present CH_2O/O_2 mechanism.

agreement of the current model predictions and the experimental data is excellent. Figure 16 shows the time history of CH_2O concentration under the shock tube conditions of Hidaka et al. [20]. Buxton and Simpson [126] measured the production rates of CO during high-temperature formaldehyde pyrolysis experiments in a shock tube. The present CH_2O/O_2 mechanism reproduces the production rates very well as illustrated in Fig. 17.

To the best of our knowledge, the only published experimental study that reported profile data for formaldehyde flames is the low-pressure work by Vandooren et al. [127], who investigated the structure of a lean CH_2O/O_2 flame using molecular beam sampling coupled with mass spectrometric analysis. Unfortunately, experimental uncertainties are quite large. For example, the error limits in HCO and HO_2 concentrations were reported as ±25% [127], and the carbon and hydrogen balances from the experimental profiles disagree with the quoted initial inputs by ±10% and ±20%, respectively [9]. The experimental flame temperature profile was used as input in the present PREMIX calculations. Species profiles predicted by the current updated CH_2O mechanism are in reasonable agreement with the experimental measurements, as shown in Fig. 18. Additional experimental flame studies would be useful for mechanism verification and/or modification.

Predictions using the current mechanism were also compared with the APFR studies from [9]. As shown

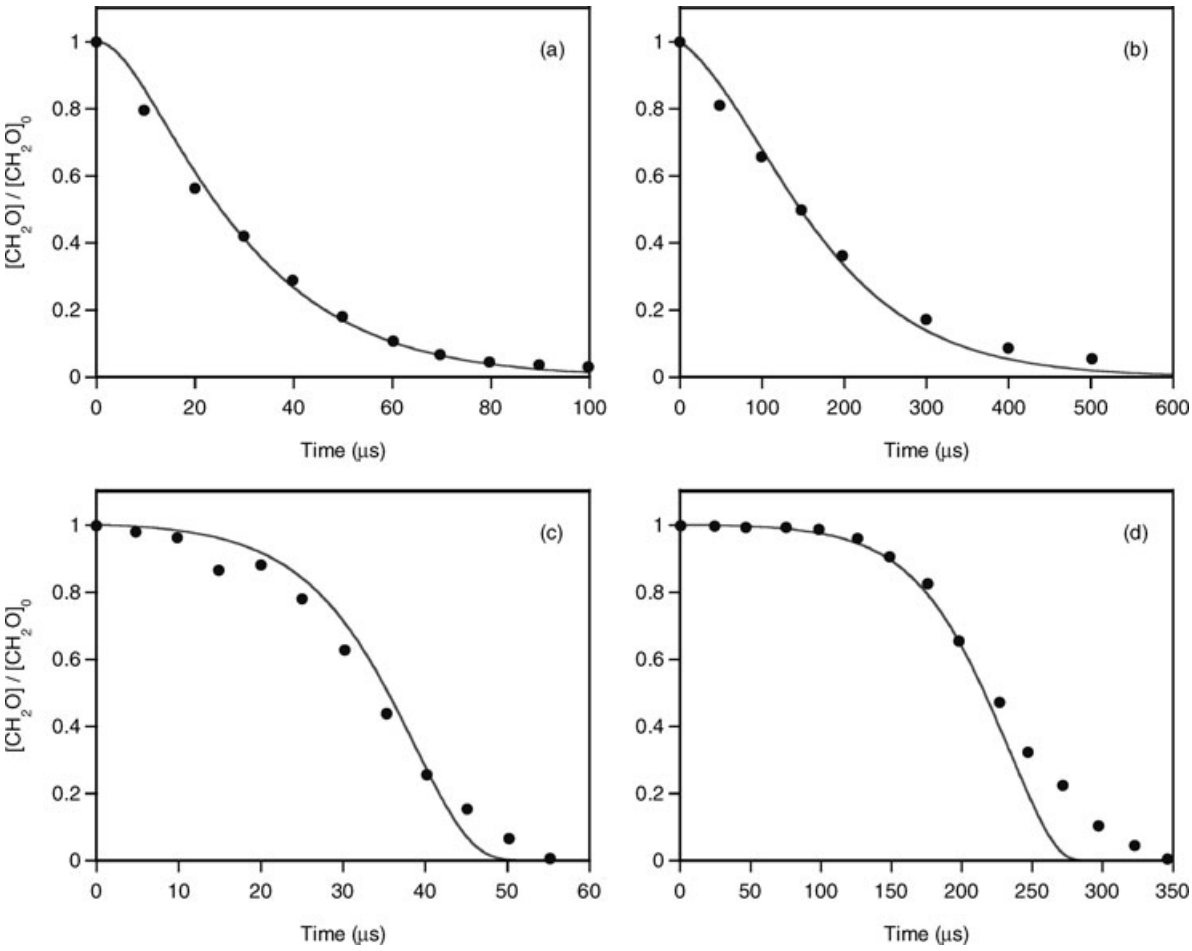

Figure 16 Normalized CH_2O concentration profiles for CH_2O/O_2/Ar mixtures in a shock tube. Initial conditions for (a) are 4.0% CH_2O with balance Ar at 1805 K and 2.81 atm; for (b) 0.01% CH_2O with balance Ar at 1907 K and 2.64 atm; for (c) 1.0% CH_2O, 4.0% O_2 with balance Ar at 1583 K and 2.16 atm; for (d) 1.0% CH_2O, 1.0% O_2 with balance Ar at 1414 K and 1.75 atm. Symbols represent experimental data of Hidaka et al. [20], and lines represent predictions of the present CH_2O/O_2 mechanism.

in Fig. 19, the predictions are in excellent agreement with the measured profiles of stable species concentrations. The comparison in Fig. 20 demonstrates that the present mechanism reproduces the new VPFR experimental measurements reported here very well. Tabulation of the initial conditions and results for the measurements shown in Fig. 20 are supplied as a supplemental file at http://www.interscience.wiley.com/jpages/0538-8066/suppmat/.

Figure 21 illustrates the most sensitive reactions for formaldehyde oxidation in a flow reactor [9] and for formaldehyde pyrolysis under the shock tube conditions of Hidaka et al. [20]. For both cases, the sensitivity coefficient of a reaction is defined as $\partial \ln Y / \partial \ln k$, where k is the rate constant of the reaction and Y is the mass fraction of CH_2O. The calculation results are reported for conditions when 50% of the initial CH_2O concentration has been consumed under constant pressure and constant volume assumption for the flow reactor and shock tube cases, respectively. Formaldehyde oxidation in the flow reactor is very sensitive to the abstraction reaction with HO_2 and to the two competitive HCO reactions (R24) and (R25). The sensitivity coefficients of these two reactions are almost equal but of opposite sign. Consequently, CH_2O oxidation in the flow reactor is not sensitive to the absolute rate constant of either reaction but rather to the ratio k_{24}/k_{25}, as explained above. Formaldehyde pyrolysis is very sensitive to the fuel decomposition reactions (R34) and (R35) and to the abstraction reaction (R36), where the H atom mainly comes from the HCO dissociation, i.e., reaction (R24). A majority of HCO are generated from

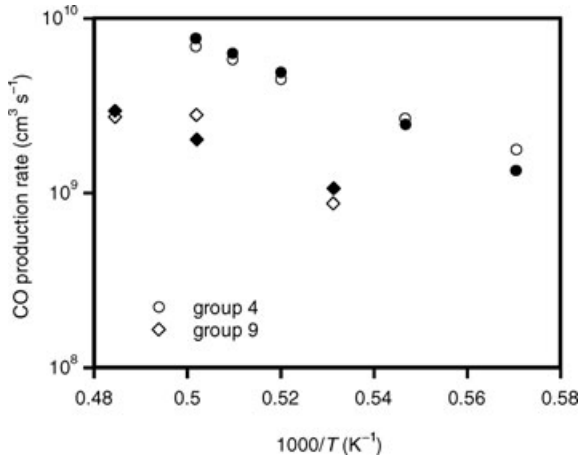

Figure 17 CO production rate during CH_2O pyrolysis in a shock tube. Initial conditions of group 4 are 1.3% CH_2O with balance Ar at 0.6–0.8 atm. Initial conditions of group 9 are 0.05% CH_2O with balance Ar at 3.2–3.5 atm. Open symbols represent the experimental data of Buxton and Simpson [126], and solid symbols represent predictions of the present CH_2O/O_2 mechanism.

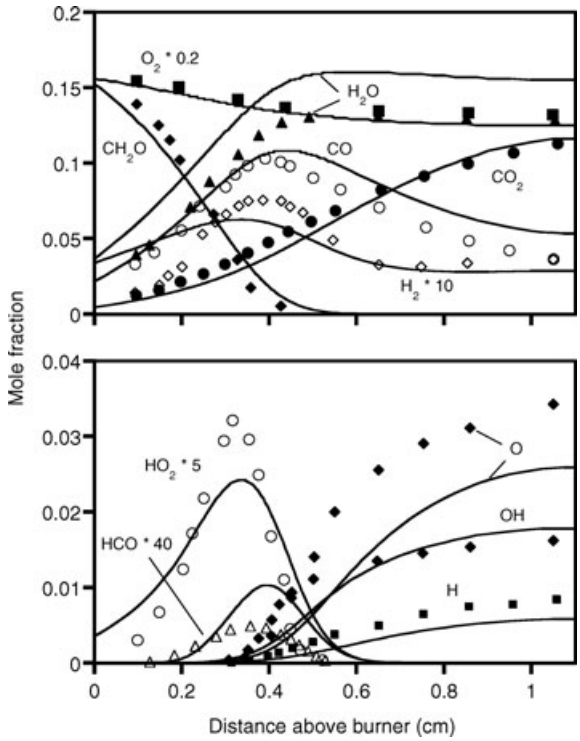

Figure 18 Species profiles in a CH_2O/O_2 burner-stabilized flame. Initial conditions are 17.9% CH_2O with 82.1% O_2 at 300 K and 0.03 atm. Symbols represent the experimental data of Vandooren et al. [127], and lines represent predictions of the present CH_2O/O_2 mechanism. The predictions are shifted by −0.1 cm to match the fuel profile data.

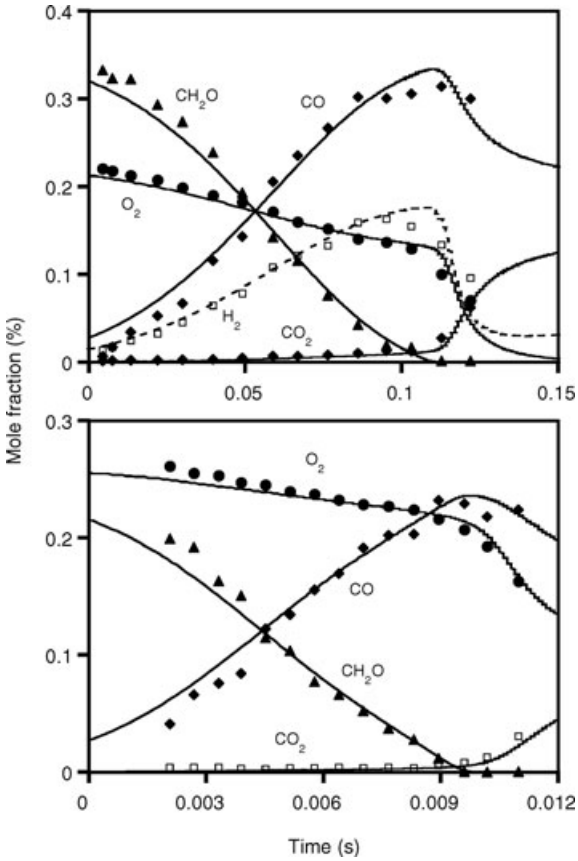

Figure 19 Reaction profiles of $CH_2O/O_2/N_2$ mixtures in an atmospheric flow reactor. Initial conditions: $CH_2O = 0.348\%$, $O_2 = 0.223\%$ with balance N_2 at 945 K (top); $CH_2O = 0.243\%$, $O_2 = 0.261\%$ with balance N_2 at 1095 K (bottom). Symbols represent the experimental data of Hochgreb and Dryer [9], and lines are predictions of the present CH_2O/O_2 mechanism. Model predictions are time shifted to match the 50% fuel consumption point.

reaction (R36). Species flux analysis reveals that the formaldehyde pyrolysis can be represented by the following five reactions:

$$HCO + M = H + CO + M \quad \text{(R24)}$$

$$HCO + H = H_2 + CO \quad \text{(R26)}$$

$$CH_2O + M = H + HCO + M \quad \text{(R34)}$$

$$CH_2O + M = H_2 + CO + M \quad \text{(R35)}$$

$$CH_2O + H = HCO + H_2 \quad \text{(R36)}$$

CH_3OH/O_2 Mechanism

Predictions using the present oxidation mechanism have been compared with the experimental targets

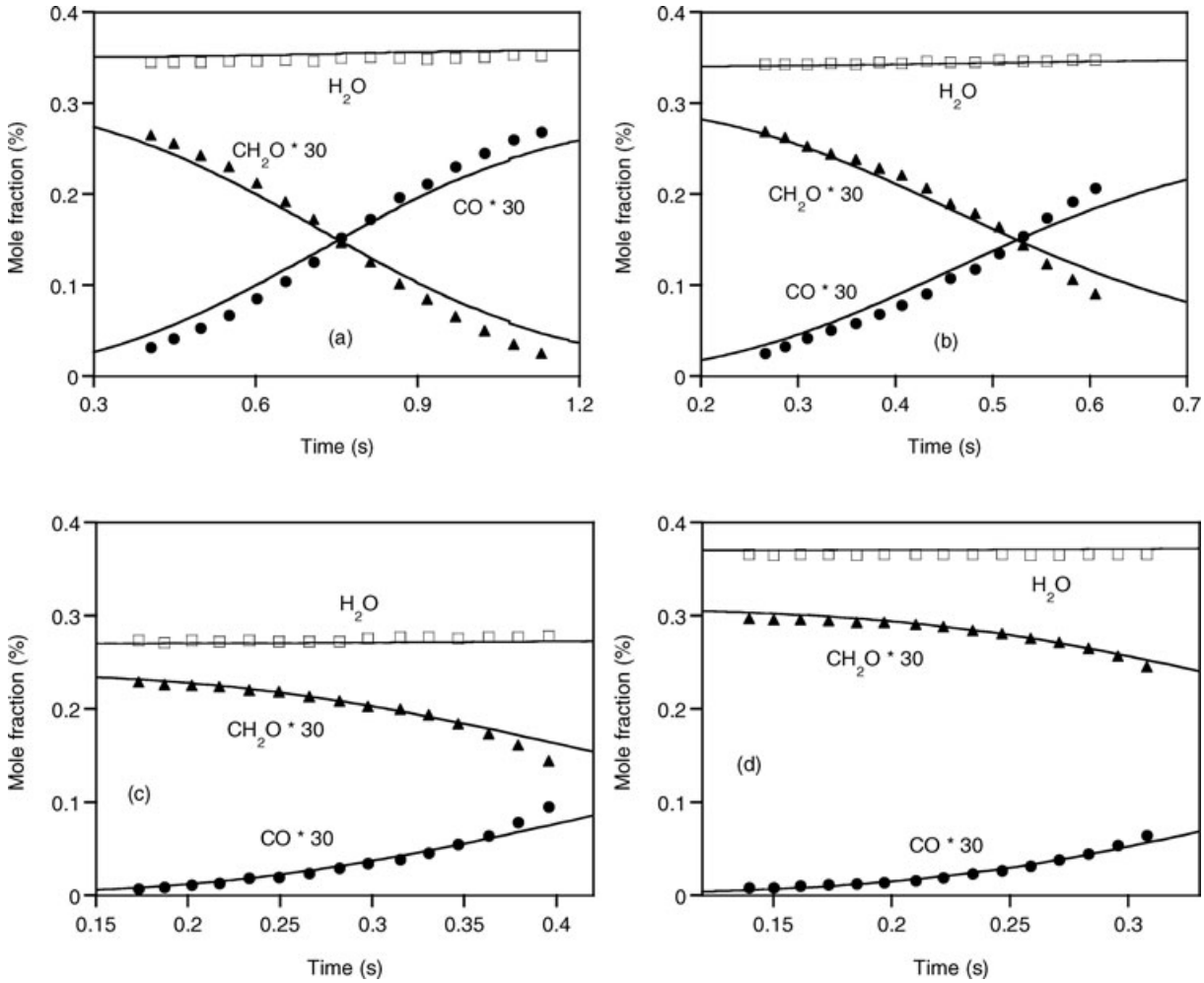

Figure 20 Reaction profiles of $CH_2O/H_2O/O_2/N_2$ mixtures in a flow reactor. Initial conditions are (a) CH_2O 100 ppm, O_2 1.5%, H_2O 0.35% with balance N_2 at 852 K and 6.0 atm; (b) CH_2O 100 ppm, O_2 2.0%, H_2O 0.34% with balance N_2 at 902 K and 3.0 atm; (c) CH_2O 80 ppm, O_2 1.8%, H_2O 0.27% with balance N_2 at 924 K and 2.5 atm; (d) CH_2O 103 ppm, O_2 2.0%, H_2O 0.37% with balance N_2 at 948 K and 1.5 atm. Symbols represent the present experimental data, and lines are predictions of the present CH_2O/O_2 mechanism. Model predictions are time shifted to match the 50% ((a) and (b)) or 90% ((c) and (d)) fuel consumption point.

utilized in the developing the mechanism of Held and Dryer [4]. The model performance over a wide array of experimental conditions was found to be better than that of the original mechanism, especially for ignition delay and premixed flame cases. Representative comparisons are shown in Figs. 22–25.

Comparisons in Figs. 22 and 23 demonstrate that the predictions are in good agreement with the species time history measurements in flow reactors [28, 128, 129]. Predictions also compare well with shock tube ignition delay data, as shown in Fig. 24. In the shock tube study of Bowman [130], the ignition delay time, τ, was approximated by the time at which the product of CO and O concentrations reached its maximum. The ignition delay time calculated using the original methanol mechanism, which is systematically shorter than the experimental observations especially at low temperatures, is also presented in Fig. 24. Prediction comparisons with laminar premixed flame speeds at three different initial temperatures also demonstrate good agreement with the experimental data [131] and noticeable improvement over comparisons generated using the original mechanism (Fig. 25).

Sensitivity analysis was performed using the present CH_3OH/O_2 mechanism for three representative situations: the mass fraction time history of CH_3OH in a

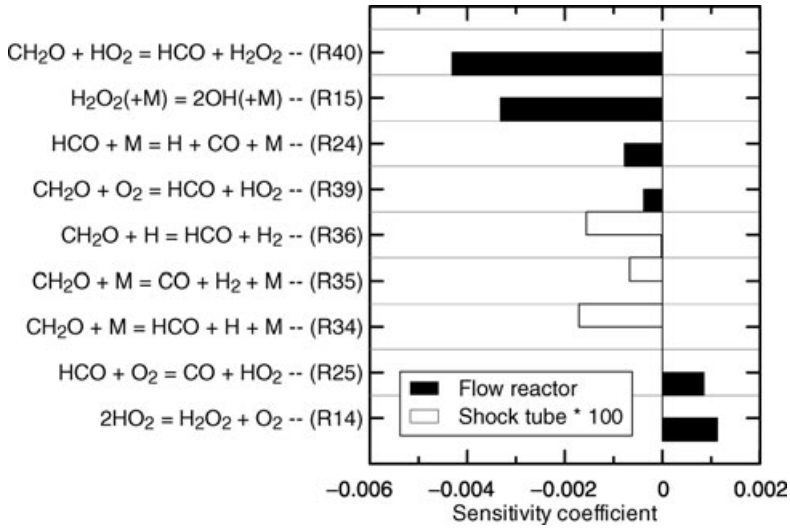

Figure 21 Sensitivity coefficients for flow reactor [9] and shock tube [20] cases. Initial conditions: 0.348% CH_2O, 0.223% O_2 with balance N_2 at 1 atm and 945 K [9]; 100 ppm CH_2O with balance Ar at 2.64 atm and 1907 K [20]. The sensitivity coefficient is calculated by using the present CH_2O/O_2 mechanism, and taken at the time when 50% CH_2O has been consumed. The sensitivity coefficient for shock tube case has been multiplied by 100.

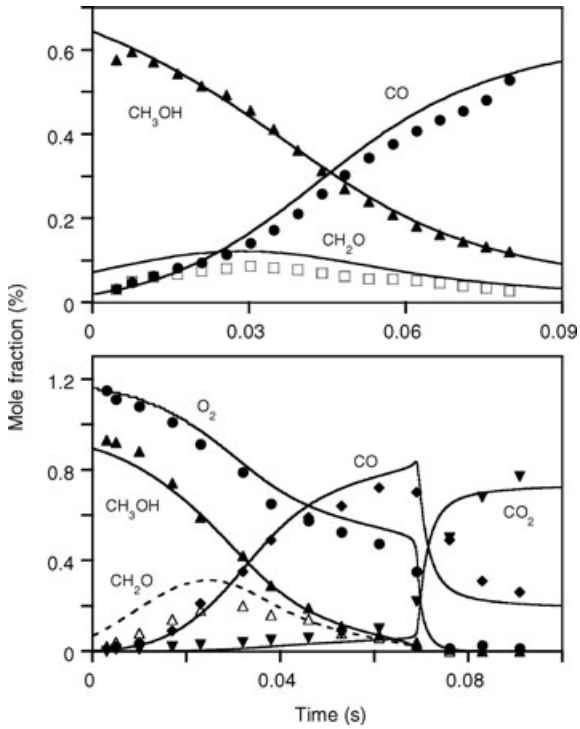

Figure 22 Reaction profiles of $CH_3OH/O_2/N_2$ mixtures in an atmospheric flow reactor. Initial conditions: $CH_3OH = 0.735\%$, $O_2 = 0.649\%$ with balance N_2 at 1000 K (top); $CH_3OH = 0.93\%$, $O_2 = 1.18\%$ with balance N_2 at 1031 K (bottom). Symbols represent the experimental data of Aronowitz et al. [128] (top) and Norton and Dryer [129] (bottom). Lines are predictions of the present CH_3OH/O_2 mechanism. Model predictions are time shifted to match the 50% fuel consumption point.

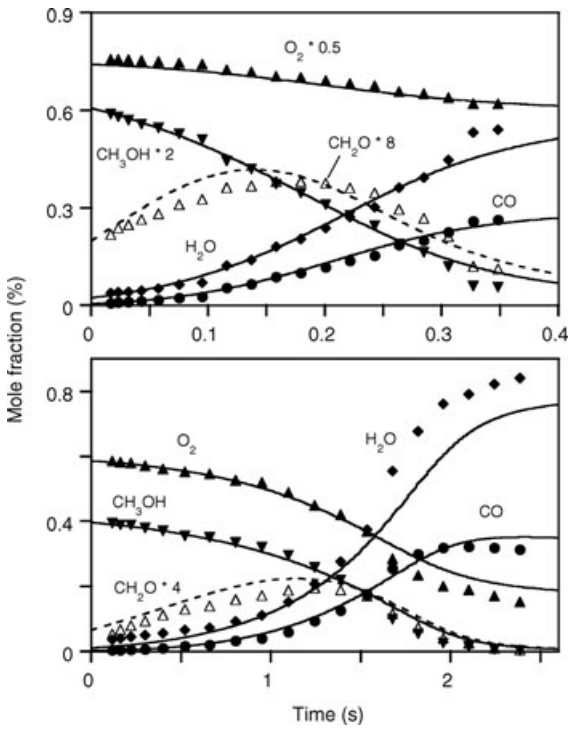

Figure 23 Reaction profiles of $CH_3OH/O_2/N_2$ mixtures in a flow reactor. Initial conditions: $CH_3OH = 0.333\%$, $O_2 = 1.5\%$ with balance N_2 at 970 K and 2.5 atm (top); $CH_3OH = 0.415\%$, $O_2 = 0.6\%$ with balance N_2 at 783 K and 15.0 atm (bottom). Symbols represent the experimental data of Held [28]. Lines are predictions of the present CH_3OH/O_2 mechanism. Model predictions are time shifted to match the 50% fuel consumption point.

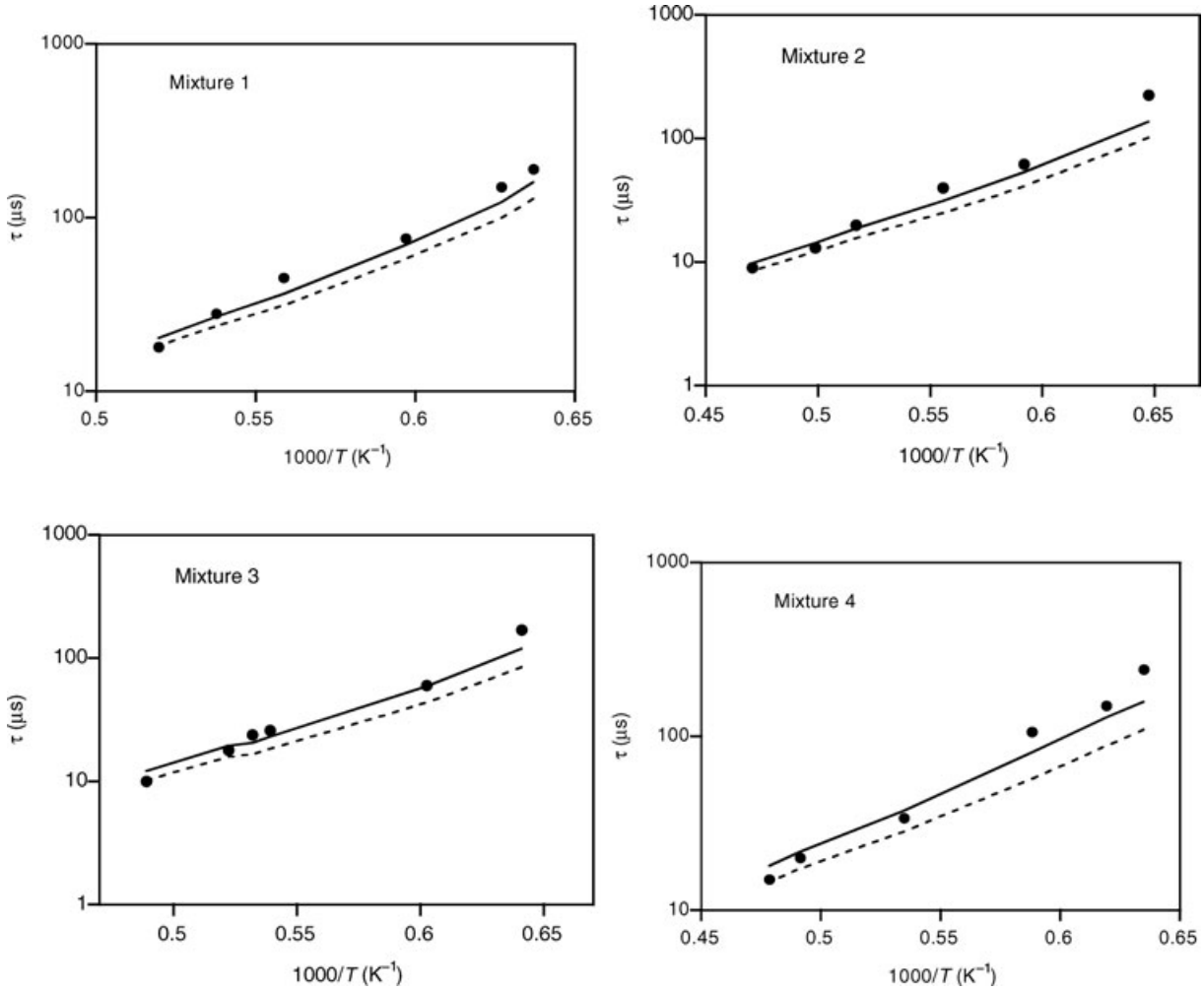

Figure 24 Ignition delay times of $CH_3OH/O_2/Ar$ mixtures in a shock tube. Initial conditions for mixture 1 are 2.0% CH_3OH, 4.0% O_2 with balance Ar at 1.2–1.7 atm; for mixture 2, 1.0% CH_3OH, 2.0% O_2 with balance Ar at 2.9–3.6 atm; for mixture 3, 0.75% CH_3OH, 1.5% O_2 with balance Ar at 3.8–4.5 atm; for mixture 4, 1.0% CH_3OH, 1.0% O_2 with balance Ar at 2.9–3.3 atm. τ is defined as the time when the product of CO and O concentrations reaches its maximum value. Symbols represent the experimental data of Bowman [130], solid lines represent predictions of the present CH_3OH/O_2 mechanism, and dashed lines represent the predictions of Held and Dryer [4].

VPFR case at 2.5 atm [28], the ignition delay time under shock tube conditions of Bowman [130], and the laminar flame speed of CH_3OH/air mixture at $\phi = 1.1$ [131]. The most sensitive reactions found are shown in Fig. 26 along with their sensitivity coefficients. As can be seen, HO_2 and H_2O_2 have critical influence on the overall reaction rate under flow reactor conditions. The fuel concentration is most sensitive to the abstraction reaction with HO_2,

$$CH_3OH + HO_2 = CH_2OH + H_2O_2 \qquad (R82)$$

although this reaction does not significantly contribute directly to the fuel destruction. Hydrogen peroxide (H_2O_2) is mainly formed via reaction (R82) and

$$2HO_2 = H_2O_2 + O_2 \qquad (R14)$$

Once formed, hydrogen peroxide primarily undergoes thermal decomposition,

$$H_2O_2\ (+M) = 2OH \qquad (R15)$$

accounting for more than 90% of the total OH production. Flux analysis shows that more than 70% of the fuel is consumed by abstraction reactions with OH,

$$CH_3OH + OH = CH_3O + H_2O \qquad (R78)$$

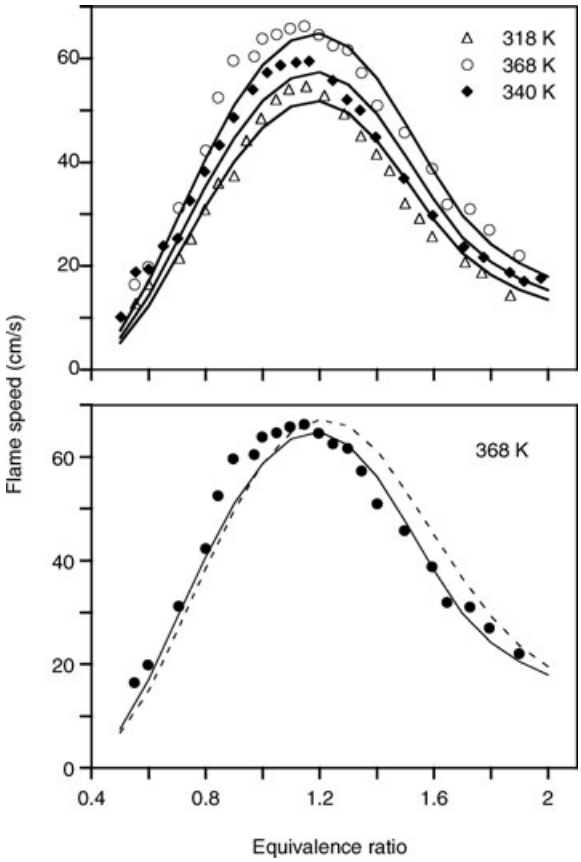

Figure 25 Atmospheric laminar flame speeds of CH_3OH/air mixtures at different initial temperatures (318, 340, and 368 K). Symbols represent the experimental data of Egolfopoulos et al. [131], solid lines are predictions of present CH_3OH/O_2 mechanism, and the dashed line in the bottom figure shows the predictions of Held and Dryer [4].

$$CH_3OH + OH = CH_2OH + H_2O \qquad (R79)$$

to which the CH_3OH/O_2 system also exhibits large sensitivity. In addition to the fuel abstraction reactions with HO_2, OH, and H, the ignition delay time is also very sensitive to the fuel dissociation reaction (R72). For the laminar premixed flame case, H atom has a critical influence on the flame speed because H atom plays an important role in radical pool buildup and has large diffusivity. As can be seen from Fig. 26, the flame speed is mainly sensitive to the chain-branching reaction,

$$H + O_2 = O + OH \qquad (R1)$$

and to the formyl radical decomposition reaction,

$$HCO + M = H + CO + M \qquad (R24)$$

which was found through reaction flux analysis to be the main source of H atoms in the system [4], along with

$$CO + OH = CO_2 + H \qquad (R23)$$

CONCLUSIONS

The detailed CH_3OH oxidation mechanism of Held and Dryer [4] has been updated using recently published rate constants and thermochemical data for OH, HO_2, and CH_2OH to yield a new, comprehensive C_1 kinetic mechanism. The mechanism was developed in a hierarchical manner, which included substantial validation of submechanism components through comparisons of predictions against experiments involving H_2, CO, and CH_2O as the initial fuel. Modifications to rate correlations for reactions (R23) and (R24), which are responsible for the formation of CO_2 and CO, were extensively investigated, and new rate correlations for reactions (R23) and (R24) were developed based upon weighted least-square fits of available experimental measurements. The new correlations significantly improve reproductions of experimental results over temperature ranges of most significance in modeling premixed laminar flame speeds.

Predictions using the present C_1 mechanism were compared against a wide range of experimental conditions (300–3000 K, 0.15–9.6 atm, $\phi = 0.4$–6.1 for CO oxidation; 300–2150 K, 0.03–12.0 atm, $\phi = 0.005$, pyrolysis for CH_2O; 300–2200 K, 1.0–20 atm, $\phi = 0.05$–6.0 for CH_3OH oxidation) found in laminar premixed flames, shock tubes, and flow reactors for CO, CH_2O, and CH_3OH combustion. Very good agreement of model predictions with the experimental measurements demonstrates that the updated C_1 mechanism is a comprehensive model for CO, CH_2O, and CH_3OH combustion. The current mechanism in an electronic form compatible with CHEMKIN is provided as a supplemental file at http://www.interscience.wiley.com/jpages/0538-8066/suppmat/.

The authors thank Mr. Paul Michniewicz for his assistance in performing the VPFR experiments. We also wish to thank Prof. C-J. Sung for an advance copy of he and his co-authors' manuscript [119] prior to publication.

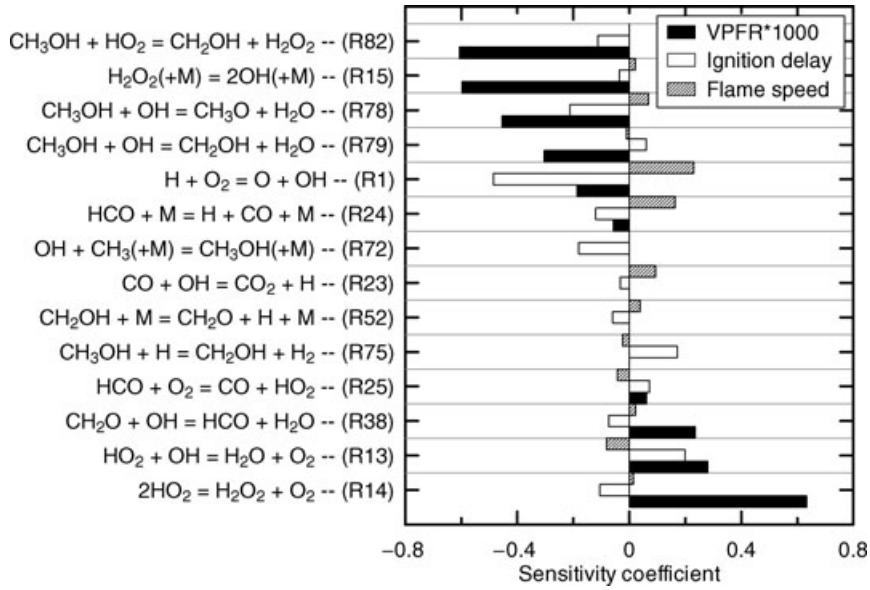

Figure 26 Sensitivity coefficients for flow reactor [28], shock tube [130], and laminar premixed flame [131] cases. Initial conditions are 0.333% CH_3OH, 1.5% O_2 with balance N_2 at 970 K and 2.5 atm [28]; 0.75% CH_3OH, 1.5% O_2 with balance Ar at 4.1 atm and 1660 K [130]; and CH_3OH/air mixture with equivalence ratio of 1.1 at 1.0 atm and 340 K [131]. The sensitivity coefficient for the flow reactor case is taken at the time when 50% CH_3OH has been consumed, and has been multiplied by 1000, except that multiplied by 250 for reactions $H_2O_2 (+M) = 2OH (+M)$ (R15) and $CH_3OH + HO_2 = CH_2OH + H_2O_2$ (R82). The shock tube ignition delay time is defined as the time when the product of CO and O concentrations reaches its maximum.

BIBLIOGRAPHY

1. Westbrook, C. K.; Dryer, F. L. Proc Combust Inst 1981, 18, 749.
2. Westbrook, C. K; Dryer, F. L. Prog Energy Combust Sci 1984, 10, 1.
3. Glassman, I. Combustion, 3rd ed.; Academic Press: New York; 1996.
4. Held, T. J.; Dryer, F. L. Int J Chem Kinet 1998, 30, 805.
5. Dryer, F. L.; Chaos, M.; Zhao, Z.; Stein, J. N.; Alpert, J. Y.; Homer, C. J. Combust Sci Technol 2007, 179 (in press).
6. Astbury, G. R.; Hawksworth, S. J. Proceedings of the International Conference on Hydrogen Safety, Pisa, Italy, 2005.
7. Yetter, R. A.; Rabitz, H.; Dryer, F. L. Combust Sci Technol 1991, 79, 129.
8. Yetter, R. A.; Dryer, F. L.; Rabitz, H. Combust Sci Technol 1991, 79, 97.
9. Hochgreb, S.; Dryer, F. L. Combust Flame 1992, 91, 257.
10. Kim, T. J.; Yetter, R. A.; Dryer, F. L. Proc Combust Inst 1994, 25, 759.
11. Norton, T. S.; Dryer, F. L. Int J Chem Kinet 1990, 22, 219.
12. Held, T. J.; Dryer, F. L. Proc Combust Inst 1994, 25, 901.
13. Mueller, M. A. Ph.D. Thesis; Department of Mechanical and Aerospace Engineering, Princeton University, Princeton, NJ, 2000.
14. Mueller, M. A.; Yetter, R. A.; Dryer, F. L. Int J Chem Kinet 1999, 31, 113.
15. Mueller, M. A.; Yetter, R. A.; Dryer, F. L. Proc Combust Inst 1998, 27, 177.
16. Mueller, M. A.; Kim, T. J.; Yetter, R. A.; Dryer, F. L. Int J Chem Kinet 1999, 31, 705.
17. Mueller, M. A.; Yetter, R. A.; Dryer, F. L. Int J Chem Kinet 2000, 32, 317.
18. Li, J.; Zhao. Z.; Kazakov, A.; Dryer, F. L. Int J Chem Kinet 2004, 36, 565.
19. Friedrichs, G.; Herbon, J.T.; Davidson, D. F.; Hanson, R. K. Phys Chem Chem Phys 2002, 4, 5778.
20. Hidaka, Y.; Taniguchi, T.; Tanaka, H.; Kamesawa, T.; Inami, K.; Kawano, H. Combust Flame 1993, 92, 365.
21. Eiteneer, B.; Yu, C. L.; Goldenberg, M.; Frenklach, M. J. Phys Chem A 1998, 102, 5196.
22. Friedrichs, G.; Davidson, D. F.; Hanson, R. K. Int J Chem Kinet 2004, 36, 157.
23. Huang, Y.; Sung, C. J.; Eng, J. A. Combust Flame 2004, 139, 239.
24. DeSain, J. D.; Jusinski, L. E.; Ho, A. D.; Taatjes, C. A. Chem Phys Lett 2001, 347, 79.
25. Senosiain, J. P.; Musgrave, C. B.; Golden, D. M. Int J Chem Kinet 2003, 35, 464.
26. Li, J. Ph.D. thesis; Department of Mechanical and Aerospace Engineering, Princeton University, Princeton, NJ, 2004.
27. Scire, J. J. Jr., Ph.D. thesis; Department of Mechanical and Aerospace Engineering, Princeton University, Princeton, NJ, 2002.

28. Held, T. J. Ph.D. thesis; Department of Mechanical and Aerospace Engineering, Princeton University, Princeton, NJ, 1993.
29. Hochgreb, S.; Dryer, F. L. J. Phys Chem 1992, 96, 295.
30. Budavari, S.; O'Neil, M. J.; Smith, A.; Heckelman, P. E.; Kinneary, J. F. The Merck Index, 12th ed; Merck Research Laboratories, Whitehouse station, NJ; 1996.
31. Fischer, S. L.; Dryer, F. L.; Curran, H. J. Int J Chem Kinet 2000, 32, 713.
32. Held, T. J. Personal communication, 2004.
33. Ruscic, B.; Wagner, A. F.; Harding, L. B.; Asher, R. L.; Feller, D.; Dixon, D. A.; Peterson, K. A.; Song, Y.; Qian, X.; Ng, C.; Liu, J.; Chen, W.; Schwenke, D. W. J Phys Chem A 2002, 106, 2727.
34. Herbon, J. T.; Hanson, R. K.; Golden, D. M.; Bowman, C. T. Proc Combust Inst 2002, 29, 1201.
35. Hills, A. J.; Howard, C. J. J. Chem Phys 1984, 81, 4458.
36. Ruscic, B.; Pinzon, R. E.; Morton, M. L.; Srinivasan, N. K.; Su, M. -C.; Sutherland, J. W.; Michael, J. V. J Phys Chem A 2006, 110, 6592.
37. Johnson, R. D.; Hudgens, J. W. J Phys Chem 1996, 100, 19874.
38. Ruscic, B.; Boggs, J. E.; Burcat, A.; Csaszar, A. G.; Demaison, J.; Janoschek, R.; Martin, J. M. L.; Morton, M. L.; Rossi, M. J.; Stanton, J. F.; Szalay, P. G.; Westmoreland, P. R.; Zabel, F.; Berces, T. J Phys Chem Ref Data 2005, 34, 573.
39. Gordon, S.; McBride, B. J. NASA SP-273, 1971.
40. Dryer, F. L. Ph.D. thesis; Department of Mechanical and Aerospace Engineering, Princeton University, Princeton, NJ, 1972.
41. Warnatz, J. In Combustion Chemistry; Gardiner, W. C., Jr., (Ed.); Springer-Verlag: New York, 1984.
42. Miller, J. A.; Kee, R. J.; Westbrook, C. K. Annu Rev Phys Chem 1990, 41, 345.
43. Zhao, Z.; Li, J.; Kazakov, A.; Dryer, F. L. Int J Chem Kinet 2005, 37. 282.
44. Yu, C. L. Ph.D. thesis; Department of Materials Science and Engineering, Pennsylvania State University, 1996.
45. Troe, J. Proc Combust Inst 1998, 27, 167.
46. Zhu, R. S.; Diau, E. G. W.; Lin, M. C.; Mebel, A. M. J Phys Chem A 2001, 105, 11249.
47. Smith, G. P.; Golden, D. M.; Frenklach, M.; Moriarty, N. W.; Eiteneer, B.; Goldenberg, M.; Bowman, C. T.; Hanson, R. K.; Song, S.; Gardiner, W. C., Jr.; Lissianski, V. V.; Qin, Z. (1999). Available at http://www.me.berkeley.edu/gri_mech/.
48. McLean, I. C.; Smith, D. B.; Taylor, S. C. Proc Combust Inst 1994, 25, 749.
49. Ravishankara, A. R.; Thompson, R. L. Chem Phys Lett 1983, 99, 377.
50. Wooldridge, M. S.; Hanson, R. K.; Bowman, C. T. Proc Combust Inst 1994, 25, 741.
51. Wooldridge, M. S.; Hanson, R. K.; Bowman, C. T. Int J Chem Kinet 1996, 28, 361.
52. Westenberg, A. A.; deHaas, N. J. Chem Phys 1973, 58, 4061.
53. Vandooren, J.; Peeters, J.; Van Tiggelen, P. J. Proc Combust Inst 1975, 15, 745.
54. Lissianski, V.; Yang, H.; Qin, Z.; Mueller, M. R.; Shin, K. S.; Gardiner, W. C., Jr.; Chem Phys Lett 1995, 240, 57.
55. Yu, C. L.; Wang, C.; Frenklach, M. Eastern States Section of the Combustion Institute Technical Meeting, Ithaca, NY, 1991.
56. Joshi, A. V.; Wang, H. Int J Chem Kinet 2006, 38, 57.
57. Timonen, R. S.; Ratajczak, E.; Gutman, D. J Phys Chem 1987, 91, 5325.
58. Timonen, R. S.; Ratajczak, E.; Gutman, D. J Phys Chem 1988, 92, 651.
59. Glarborg, P.; Alzueta, M. U.; Kjargaard, K.; Dam-Johansen, K. Combust. Flame 2003, 132, 629.
60. Pearson, G. S. J Phys Chem 1963, 67, 1686.
61. Schecker, H. G.; Jost, W. Ber Bunsen-Ges. Phys Chem 1969, 73, 521.
62. Browne, W. G.; Porter, R. P.; Verlin, J. D.; Clark, A. H. Proc Combust Inst 1969, 12, 1035.
63. Bowman, C. T. Combust Sci Technol 1970, 2, 161.
64. Ahumada, J. J.; Michael, J. V.; Osborne, D. T. J Chem Phys 1972, 57, 3736.
65. Baldwin, R. R.; Jackson, D.; Melvin, A.; Rossiter, B. N. Int J Chem Kinet 1972, 4, 277.
66. Wang, H. Y.; Eyre, J. A.; Dorfman, L. M. J Chem Phys 1973, 59, 5199.
67. Westbrook, C. K.; Creighton, J.; Lund, C.; Dryer, F. L. J Phys Chem 1977, 81, 2542.
68. Campbell, I. M.; Handy, B. J. J Chem Soc Faraday Trans 2 1978, 74, 316.
69. Hochanadel, C. J.; Sworski, T. J.; Ogren, P. J. J Phys Chem 1980, 84, 231.
70. Cherian, M. A.; Rhodes, P.; Simpson, R. J.; Dixon-Lewis, G. Proc Combust Inst 1981, 18, 385.
71. Cribb, P. H.; Dove, J. E.; Yamazaki, S. Combust Flame 1992, 88, 169.
72. Krasnoperov, L. N.; Chesnokov, E. N.; Stark, H.; Ravishankara, A. R. J Phys Chem A 2004, 108, 11526.
73. Hippler, H.; Kastreva, N.; Striebel, F. Phys Chem Chem Phys 2004, 6, 3383.
74. Krasnoperov, L. N. Phys Chem Chem Phys 2005, 7, 2074.
75. Hippler, H.; Kastreva, N.; Striebel, F. Phys Chem Chem Phys 2005, 7, 2077.
76. Colberg, M.; Friedrichs, G. J Phys Chem A 2006, 110, 160.
77. Irdam, E. A.; Kiefer, J. H.; Harding, L. B.; Wagner, A. F. Int J Chem Kinet 1993, 25, 285.
78. Friedrichs, G.; Davidson, D. F.; Hanson, R. K. Int J Chem Kinet 2002, 34, 374.
79. Vasudevan, V.; Davidson, D. F.; Hanson, R. K. Int J Chem Kinet 2005, 37, 98.
80. Vasudevan, V.; Davidson, D. F.; Hanson, R. K.; Bowman, C. T.; Golden, D. M. Proc Combust Inst 2007, 31, doi: 10.1016/j.proci.2006.07.017.
81. Tsang, W.; Hampson, R. F. J. Phys Chem Ref Data 1986, 15, 1087.

82. Gilbert, R. G.; Luther, K.; Troe, J. Ber Bunsen-Ges Phys Chem 1983, 87, 169.
83. Koike, T.; Kudo, M.; Maeda, I.; Yamada, H. Int J Chem Kinet 2000, 32, 1.
84. Krasnoperov, L. N.; Michael, J. V. J Phys Chem A 2004, 108, 8317.
85. Jimenez, E.; Gilles, M. K.; Ravishankara, A. R. J Photochem Photobiol A 2003, 157, 237.
86. Bott, J. F.; Cohen, N. Int J Chem Kinet 1991, 23, 1075.
87. Hessler, J. P. J Phys Chem A 1998, 102, 4517.
88. Sutherland, J. W.; Michael, J. V.; Pirraglia, A. N.; Nesbitt, F. L.; Klemm R. B. Proc Combust Inst 1986, 21, 929.
89. Michael, J. V.; Sutherland, J. W. J Phys Chem 1988, 92, 3853.
90. Sutherland, J. W.; Patterson, P. M.; Klemm, R. B. Proc Combust Inst 1990, 23, 51.
91. Cobos, C. J.; Hippler, H.; Troe, J. J Phys Chem 1985, 89, 342.
92. Hippler, H.; Troe, J.; Willner, J. J Chem Phys 1990, 93, 1755.
93. Brouwer, L.; Cobos, C. J.; Troe, J.; Dubal, H. R.; Crim, F. F. J Chem Phys 1985, 86, 6171.
94. Michael, J. V.; Su, M. C.; Sutherland, J. W.; Carroll, J. J.; Wagner, A. F. J Phys Chem A 2002, 106, 5297.
95. Baulch, D. L; Cobos, C. J.; Cox, R. A.; Esser, C.; Frank, P.; Just, Th.; Kerr, J. A.; Pilling, M. J.; Troe, J.; Walker, R. W.; Warnatz, J. J Phys Chem Ref Data 1992, 21, 411.
96. Hippler, H.; Troe, J. Chem Phys Lett 1992, 192, 333.
97. Troe, J. J Phys Chem 1975, 83, 114.
98. Westmoreland, P. R.; Howard, J. B.; Longwell, J. P.; Dean, A. M. AIChE J 1986, 32, 1971.
99. Slagle, I. R.; Sarzynski, D.; Gutman, D. J Phys Chem 1987, 91, 4375.
100. Scire, J. J.; Yetter, R. A.; Dryer, F. L. Int J Chem Kinet 2001, 33, 75.
101. Frenklach, M.; Wang, H.; Goldenberg, M.; Smith, G. P.; Golden, D. M.; Bowman, C. T.; Hanson, R. K.; Gardiner, W. C.; Lissianski, V. GRI Technical Report no. GRI-95/0058, 1995.
102. Schatz, G. C.; Wagner, A. F.; Dunning, T. H. J Phys Chem 1984, 88, 221.
103. Klemm, R. B.; Tanzawa, T.; Skolnik, E. G.; Michael, J. V. Proc Combust Inst 1981, 18, 785.
104. Felder, W.; Madronich, S. Combust Sci Technol 1986, 50, 135.
105. Tsang, W. J. Phys Chem Ref Data 1987, 16, 471.
106. Grotheer, H. H.; Riekert, G.; Walter, D.; Just, Th. J Phys Chem 1988, 92, 4028.
107. Page, M.; Lin, M. C.; He, Y.; Choudhury, T. K. J Phys Chem 1989, 93, 4404.
108. Wantuck, P. J.; Oldenborg, R. C.; Baughcum, S. L.; Winn, K. R. J Phys Chem 1987, 91, 4653.
109. Cathonnet, M.; Boettner, J. C.; James, H. J Chim Phys 1982, 79, 475.
110. Kee, R. J.; Rupley, F. M.; Miller, J. A. Technical Report SAND87-8215B, Sandia National Laboratories, Albuquerque, NM, 1987.
111. Burcat, A., Technion Aerospace Engineering, Report #867, 2001.
112. Wang, H.; Laskin, A.; Djurisic, Z. M.; Law, C. K.; Davis, S. G.; Zhu, D. L. Eastern States Section of the Combustion Institute Fall Technical Meeting, 1999, 129, Raleigh, NC.
113. Lutz, A. E.; Kee, R. J.; Miller, J. A. Technical Report SAND87-8248, Sandia National Laboratories, Albuquerque, NM, 1987.
114. Kee, R. J.; Grcar, J. F.; Smooke, M. D.; Miller, J. A., Technical Report SAND85-8240, Sandia National Laboratories, Albuquerque, NM, 1985.
115. Kee, R. J.; Dixon-Lewis, G.; Warnatz, J.; Coltrin, M. E.; Miller, J. A. Technical Report SAND86-8246, Sandia National Laboratories, Albuquerque, NM, 1986.
116. Dean, A. M.; Steiner, D. C.; Wang, E. E. Combust Flame 1978, 32, 73.
117. Gardiner, W. C. jr.; McFarland, M.; Morinaga, K.; Takeyama, T.; Walker, B. F. J Phys Chem 1971, 75, 1504.
118. Mueller, M. A.; Yetter, R. A.; Dryer, F. L. Int J Chem Kinet 1999, 31, 705.
119. Mittal, G.; Sung, C-J.; Yetter, R. A. Int J Chem Kinet 2006, 38, 516.
120. Sivaramakrishnan, R.; Comandini, A.; Tranter, R. S.; Brezinsky, K. 6th International Conference on Chemical Kinetics, Gaithersburg, MD, July 25–29, 2005.
121. Kazakov, A.; Chaos, M.; Zhao, Z.; Dryer, F. L. J Phys Chem A 2006, 110, 7003.
122. Mittal, G.; Sung, C-J. Combust Sci Technol (in press) (online at http://mae1.cwru.edu/mae/Pages/Facilities/CDL/RCM_CST_Mittal&Sung.pdf).
123. Sivaramakrishnan, R.; Comandini, A.; Tranter, R. S.; Brezinsky, K; Davis, S. G.; Wang, H. Proc Combust Inst 2007, 31; doi: 10.1016/j.proci.2006.08.057.
124. Mittal, G.; Sung, C. J.; Fairweather, M.; Tomlin, A. S.; Griffiths, J. F.; Hughes, K. J. Proc Combust Inst 2007, 31; doi: 10.1016/j.proci.2006.07.068.
125. Kappel, C-H.; Luther, K.; Troe, J. Phys Chem Chem Phys 2002, 4, 4392.
126. Buxton, J. P.; Simpson, C. J. S. M. Chem Phys Lett 1986, 128, 577.
127. Vandooren, J.; Oldenhove de Guertechin, L.; Van Tiggelen, P. J Combust Flame 1986, 64, 127.
128. Aronowitz, D.; Santoro, R. J.; Dryer, F. L.; Glassman, I. Proc Combust Inst 1979, 17, 633.
129. Norton, T. S.; Dryer, F. L. Combust Sci Technol 1989, 63, 107.
130. Bowman, C. T. Combust Flame 1975, 25, 343.
131. Egolfopoulos, F. N.; Du, D. X.; Law, C. K. Combust Sci Technol 1992, 83, 33.
132. Dean, A. M.; Johnson, R. L.; Steiner, D. C. Combust Flame 1980, 37, 41.